Imperial College London

Department of Physics

Coleman-de Luccia Instantons with Gravity

Author:

Herodotos Herodotou

Supervisor:

Prof. Arttu Rajantie

Submitted in partial fulfillment of the requirements for the MSc degree in Quantum Fields and Fundamental Forces of Imperial College London

September 2021

Acknowledgements

I would like to express my deep gratitude to my supervisor, professor Arttu Rajantie, for his continuous guidance and support during the development of this thesis. Of course, I cannot neglect thanking my family and friends for their spiritual support and encouragement, not only throughout the writing of this thesis, but for the whole period of my studies.

Contents

List of figures

Abstract

This thesis presents the way to calculate the probability of a false vacuum decay by computing Coleman-de Luccia (CdL) bounce solutions (instantons) in a polynomial potential. We calculate these solutions by using the shooting method. First, these solutions are calculated in a flat spacetime and then, they are computed in a curved spacetime. In the latter case, the calculations are performed including the effect of the bounce backreaction on the metric and with a fixed de Sitter background. The results indicate that when we have a polynomial potential, there are no CdL solutions above a false-vacuum critical potential and the Hawking-Moss solution (constant solution) dominates. We also compare the bounce solutions with and without gravitational back-reaction and we conclude that when the energy density difference ΔV is much larger of the value of the false-vacuum potential V_0, background fixed approximation is not a good approximation and we should include dynamical gravity. It is vital to understand and calculate bounce solutions with dynamical gravity since the depth of the Standard Model effective potential is large so the energy density difference is also large. Therefore, we should not assume that the metric is fixed since we will ignore some new phenomena.

Chapter 1

Introduction

1.1 Vacuum Instability

The Standard Model is one of the excellent achievements of the last century. This theory describes three of the four known fundamental forces (the electromagnetic, weak, and strong interactions, and not including gravity) and all known elementary particles in the universe. Many experiments have shown through time that it accurately reproduces the world as we see it. However, it leaves some phenomena unexplained so this is not the end of the story.

The vacuum ('empty space') is the space in the absence of matter. Before the discovery of special relativity by Einstein, scientists believed that there was an invisible substance called 'luminiferous aether' instead of truly vacuum. Early theories stated that this aether was a medium through which light propagated. However, the results of the Michelson–Morley experiment proved that the aether is conclusively absent and light is a wave in the electromagnetic field. Later, a model of the vacuum as an infinite sea (Dirac sea) of particles having negative energy was proposed by Paul Dirac in 1930. This idea implies the existence of an anti-particle when a particle excite the negative energy and leaves a 'hole' there.

Nonetheless, these ideas were superceded by Quantum Field Theory, where the Dirac equation is quantised as a field, the field operator obeying the Dirac equation, rather than the field being the wavefunction for a particle. In the last years there have been interesting developments in quantum field theory. A field represents a quantity that is defined in each point in spacetime. A classical field can be either scalar, i.e. each point is associated with a number (e.g. temperature), or vector (e.g. electromagnetic field). In quantum field theory there is another type of field, the spinor field. In contrast with particles, which have a finite number of degrees of freedom, the fields have infinite degrees of freedom, at least one for every point in space. In this theory, particles are excitations of a set of fundamental fields, i.e. a small, localised packet of non-zero energy that can move about in space.

A classical field theory can have two homogeneous stable equilibrium states with different energy densities. The state of smaller energy density, which is the global minimum of energy, is always stable but the other state is not. We call the former a true vacuum state and the latter a false vacuum state. Although, in classical physics, the false vacuum state appears stable, in quantum physics, it becomes unstable through barrier penetration and given the right conditions it collapses into the true vacuum state. Classically, we need to give sufficient energy to an object in order to pass over the top of a potential barrier. However, in quantum mechanics, the object may disappear on one side and reappear on the other side without being given sufficient energy to pass over it. This process, which is called 'quantum tunnelling', depends exponentially on the barrier height and barrier width and one of its cause is the radioactive decay.

Observations illustrate that our universe is in the false vacuum, at least according to the Standard Model. Nonetheless, in any second, a catastrophic event might happen. There is a tiny probability that the false vacuum state of some part of the universe may decay to a true vacuum state. Worth note, that the most

common theory that describes this decay is called bubble nucleation. This theory states that if a small region of the universe by chance reached a more stable vacuum, this bubble would spread with almost the speed of light and it would convert false vacuum into true.

In this thesis, at first, we will study vacuum decay without gravity and then with gravity which add a thermal component to the decay of the vacuum. This component might give the vacuum sufficient energy to pass over the top of a barrier. Therefore, there are different ways for a decay to occur: entirely thermal effects, entirely quantum tunnelling, or a combination of the two.

When Higgs boson was discovered in 2012 [1, 2], many questions raised about the relation of it with the stability of the electroweak vacuum. Before the discovery of the Higgs boson, some authors suggested that the electroweak vacuum might be metastable [3]. However, when the Higgs mass ($M_h = 125.09 \pm 0.25$ GeV) and the top quark mass ($M_t = 173.21$ GeV) were discovered, people started believing that the electroweak vacuum can in fact decay via the nucleation of bubbles of true vacuum in the Standard Model [4, 5]. The Higgs mass is placed in a narrow region of parameter space where the electroweak vacuum is in a metastability region i.e. it is neither completely stable nor so unstable that it should have already decayed in the lifetime of the Universe [6].

Therefore, new physics may be demanded to explain the stabilization of the potential knowing from observations that no true-vacuum bubble is likely to have nucleated in our past light cone. This is consistent with the expected lifetime of the visible Universe that is longer than its age. Many phenomena in high-energy physics might arise a vacuum decay so these phenomena may be restricted due to the possibility of vacuum decay. For example, one of these phenomena is the inflation with a high Hubble rate [7, 8, 9, 10, 11].

Now, there is an interest how gravitational back-reaction affect the vacuum decay in the Standard Model. Using the thin-wall approximation, Coleman and de Lucia proved that the change from a zero-energy-density, false vacuum to a negative-energy-density, true vacuum suppress the decay rate, due to the warped geometry of the nucleated bubbles [12]. Some authors investigated this phenomenon perturbatively [13, 14] and some others investigated vacuum decay in a black-hole background and they found that a black hole can effectively occur a vacuum decay [15, 16, 17].

An easy way to manipulate vacuum decay with gravitational effects is to use polynomial model potentials. In this thesis, we use these potentials so as to get some general conclusions.

1.2 Vacuum Decay by Instanton Approach

We know that quantum tunnelling causes vacuum decay, both with and without gravity. In classical physics, the false vacuum state of Standard Model is surely stable as its barrier is at high energy scales and no natural process present in the universe has enough energy to exceed it. However, in quantum mechanics, a vacuum decay can occur since the false vacuum state is not an energy eigenstate. It is a superposition of different energy eigenstates, which evolve in time independently. Therefore, there is a tiny probability to observe the field in the true vacuum state at any point in space-time.

Now, we will show how can we compute the probability of decay of the false vacuum per unit time per unit volume, Γ/V, using the instanton approach [12, 18, 19, 20]. By insanton, we mean a classical solution to equations of motion with an action that is finite and non-zero, either in quantum mechanics or in quantum

field theory. More specifically, it is a solution to the equations of motion of the classical field theory on a Euclidean spacetime.

It is worth noted that if the universe was infinitely old, it would be in a true vacuum. However, the universe has a finite age. At the beginning of it, at the big bang, the energy per unit volume was too high so the universe was neither in the true nor in the false vacuum. Then, as the universe expanded and cooled down, it might have moved to a false vacuum instead of a true one.

Firstly, we consider the quantum field theory of a single scalar field in four-dimensional space-time,

$$S = \int d^4x \left[\frac{1}{2}(\partial_\mu \phi)^2 - U(\phi)\right], \tag{1.2.1}$$

where the $U(\phi)$ is the potential of the theory which has two local minima: the absolute minimum i.e. true vacuum, $\phi_{\rm tv}$, and the other minimum i.e. false vacuum, $\phi_{\rm fv}$. We can also define the Euclidean action as minus the analytic continuation of (1.2.1) to imaginary time,

$$S_E = \int d^4x \left[\frac{1}{2}(\partial_\mu \phi)^2 + U(\phi)\right], \tag{1.2.2}$$

with a positive-definite metric.

In the semiclassical limit (small $\hbar$), the expression of Γ/V is of the form [19],

$$\Gamma/V = A\, e^{-B/\hbar}(1 + O(\hbar)), \tag{1.2.3}$$

where A and B are coefficients that depend on the theory that we study and we can compute them using some algorithms. For instance, in the limit of small energy-density difference between the false and true vacuum, it is possible to calculate B in closed form.

At this point, we study the vacuum decay using the instanton approach which exploits the fact that the energy E of a false vacuum, which is a metastable state, can be regarded as complex. The time evolution of the amplitude squared of the wave function for such energy with complex value has the following form

$$|\psi(x,t)|^2 = |\psi(x,0)|^2 \; e^{2\mathrm{Im(E)}t}, \tag{1.2.4}$$

and we conclude that the expression of Γ/V can be estimated from the imaginary part of this energy, Im(E). As we Wick rotate time to imaginary values ($\tau = it$), the false vacuum state evolves as

$$|\psi_{\mathrm{fv}}(\tau)\rangle = \sum_n \langle n|\psi_{\mathrm{fv}}(0)\rangle \; e^{-E_n\tau}|n\rangle, \tag{1.2.5}$$

and by taking imaginary time τ to infinity, we notice that only the lowest-lying energy state, E_0, dominates the sum

$$|\psi_{\mathrm{fv}}(\tau)\rangle = \langle 0|\psi_{\mathrm{fv}}(0)\rangle \; e^{-E_0\tau}|0\rangle. \tag{1.2.6}$$

It is noteworthy that E_0 is the false vacuum state for distributions starting around the false vacuum.

Now, we can use a Euclidean functional integral and we can compute the vacuum to vacuum transition amplitude

$$|\psi_{\mathrm{fv}}(\tau)|^2 = \langle \psi_{\mathrm{fv}}(0)|e^{-\hat{H}\tau}|\psi_{\mathrm{fv}}(0)\rangle = \int_{\phi_{\mathrm{fv}}}^{\phi_{\mathrm{fv}}} D\phi e^{-S_E[\phi]} \; , \tag{1.2.7}$$

where we integrate over all configurations for ϕ with ϕ_{fv} at the boundaries. We can always evaluate this path integral by using the semi-classical approximation, which assumes that the path integral is dominated by classical solutions called

instantons, or bounces, which are stationary points of the Euclidean action

$$\int_{\phi_{\text{fv}}}^{\phi_{\text{fv}}} D\phi e^{-S_E[\phi]} \approx \sum_i \det\left[S''[\phi_i]\right]^{-1/2} e^{-S_E[\phi_i]} \ , \tag{1.2.8}$$

where ϕ_i are the aforementioned stationary points of $S_E[\phi]$ and prime on the action indicates functional derivative. This is essentially performing a 1-loop approximation of the path integral and the proof for the calculation of this integral can be found in appendix A. Coleman and Callan demonstrated that this gives the probability of the decay of a false vacuum state per unit volume per unit time [18]

$$\Gamma/V \approx \left(\frac{B}{2\pi\hbar}\right)^2 \left|\frac{\det'\left[S_E''[\phi_B]\right]}{\det\left[S_E''[\phi_{\text{fv}}]\right]}\right|^{-1/2} e^{-B/\hbar} \ , \tag{1.2.9}$$

where the coefficient B is the difference

$$B = S_E[\phi_B] - S_E[\phi_{\text{fv}}], \tag{1.2.10}$$

and ϕ_B is the stationary point that lowers the action. Thus, ϕ_B is a bounce-solution of the Euclidean equations of motion since the Euclidean equations of motion are the Euler-Lagrange equations associated with S_E. The prime on the determinant shows that all its zero values were removed. These zero values correspond to symmetries of the action, especially translations of the bounce solution around the 4D Euclidean space. There is also a negative value in this determinant which causes the energy of the vacuum being imaginary.

Chapter 2

Vacuum Decay without Gravity

2.1 Barrier Penetration in Quantum Mechanics

One way that we can calculate the probability of false vacuum decay per unit time per unit volume is by using a WKB approximation of the wave function. In ordinary quantum mechanics, it is well known that the transition rate of a particle with total energy E through a barrier in potential $U(x)$ with a minimum point x_1 and a maximum point x_2 is [21]

$$T \propto \exp\left(-2\int_{x_1}^{x_2} dx\sqrt{2(U(x)-E)}\right). \tag{2.1.1}$$

The equation of motion of this particle is

$$\frac{d^2x}{dt^2} + U'(x) = 0, \tag{2.1.2}$$

and if you multiply this expression by $\frac{dx}{dt}$ and integrate it, you will find

$$\frac{1}{2}\left(\frac{dx}{dt}\right)^2 + U(x) = E\ , \tag{2.1.3}$$

where the total energy E is the constant of the integration. Now, changing the real time to imaginary time ($\tau = it$), we have

$$2\int_{x_1}^{x_2} dx\sqrt{2(U(x)-E)} = 2\int_{x_1}^{x_2} dx\sqrt{\left(\frac{dx}{dt}\right)^2}, \tag{2.1.4}$$

and then, we change the variables of the integration

$$2\int_{\tau_1}^{\tau_2} d\tau\left(\frac{dx}{d\tau}\right)^2 = 2\int_{\tau_1}^{\tau_2} d\tau\left[\frac{1}{2}\left(\frac{dx}{d\tau}\right)^2 + U(x) - E\right]. \tag{2.1.5}$$

Since we know that Euclidean action is

$$S_E[x] = \int d\tau\left[\frac{1}{2}\left(\frac{dx}{d\tau}\right)^2 + U(x)\right], \tag{2.1.6}$$

the transition rate of the particle is

$$T \propto \exp\left[-\Big(S_E[x_B] - S_E[x_{\rm fv}]\Big)\right], \tag{2.1.7}$$

where x_B and $x_{\rm fv}$ are solutions of the associated Euler-Lagrange equation when we substitute $\tau = it$ in (2.1.2)

$$\frac{d^2x}{d\tau^2} - U'(x) = 0. \tag{2.1.8}$$

x_B is periodic and it is called the 'bounce solution' as it starts at $x_1(\tau_1) = x_1$, bounces off $x_2(\tau_2) = x_2$ and finally, it reaches x_1 again. $x_{\rm fv}$ is called the 'false-vacuum solution' and it is constant since it sits in the false vacuum for all integrated time.

We can generalize this one-dimensional process of one particle to more dimensions and more particles with N degrees of freedom, q_i. Now, we use the WKB approximation to find transition rate for a particular route $\mathbf{q}(s)$ through

the barrier

$$T \propto \exp\Bigg(-2\int_{\mathbf{q_1}}^{\mathbf{q_2}} \sqrt{\sum_i^N \left(\frac{dq_i}{ds}\right)^2}\, ds \sqrt{2(U(\mathbf{q}(s)) - E)}\Bigg). \tag{2.1.9}$$

Obviously, the route that has the dominant contribution for tunnelling is the route that produces the largest T and it has the smallest Euclidean action

$$S_E = \int d\tau \Bigg[\sum_i^N \left(\frac{1}{2}\left(\frac{dq_i}{d\tau}\right)^2 + U(\mathbf{q}(\tau))\right)\Bigg]. \tag{2.1.10}$$

In the case that there are many bounces with the same Euclidean action, we sum the contributions for of all these bounces.

2.2 Barrier Penetration in Field Theory

At this point, we correspond the previous section to the field theory problem. As we saw before, a particle can tunnel through a barrier and emerge on the other side at a point in space while the energy is conserved. The same process is true for a field. However, the field does not emerge at a point in space but in a field configuration over the spatial degrees of freedom. This field configuration is the nucleated bubble of true vacuum, and after forming it will begin to expand with almost the speed of light. We know that many authors have investigated vacuum instability in a Minkowski background [22, 23, 24]. The simplest case is a relativistic scalar field, $\phi(x)$, in flat space-time with the Euclidean action

$$S_E(\phi) = \int d^4x \left[\frac{1}{2}\partial_\mu\phi\partial^\mu\phi + V(\phi)\right], \tag{2.2.1}$$

where $x = (\tau, \mathbf{x})$. The equation of motion of the field is

$$\left(\frac{d^2}{d\tau^2} + \nabla^2\right)\phi(x) = V'(\phi), \tag{2.2.2}$$

where the prime denotes differentiation with respect to $\phi(x)$. We note that the field does not penetrate $V(\phi)$ but the potential

$$U(\phi) = \int d^3\mathbf{x} \left(\frac{1}{2}(\nabla\phi)^2 + V(\phi)\right), \tag{2.2.3}$$

since we can write the action of (2.2.1) as

$$S_E(\phi) = \int d\tau \left[\left(\int d^3\mathbf{x} \frac{1}{2}\left(\frac{d\phi}{d\tau}\right)^2\right) + \left(\int d^3\mathbf{x}\left(\frac{1}{2}(\nabla\phi)^2\right) + V(\phi)\right)\right]. \tag{2.2.4}$$

$V(\phi)$ is the potential energy density.

Generally, we should evaluate the path integral to find the probability of the decay of false vacuum including all the contributions from each solution of (2.2.2). Nonetheless, the most important contribution to path integral is the bounce that lowers the action, with other solutions giving exponentially small contributions compare to this.

The boundary conditions for the bounce are

$$\phi(\pm\infty, \mathbf{x}) \to \phi_{\text{tv}} \tag{2.2.5}$$

and

$$\frac{\partial\phi}{\partial\tau}(0, \mathbf{x}) = 0. \tag{2.2.6}$$

We have an other boundary condition

$$\phi(\tau, \pm\infty) \to \phi_{\text{fv}} \tag{2.2.7}$$

so as the Euclidean action to be finite.

Solutions of these equations are not invariant under spatial translations. However, they are invariant under four-dimensional Euclidean rotations (O(4) symmetry) i.e. the solution ϕ is a function of ρ only, where

$$\rho = \sqrt{\tau^2 + \mathbf{x}^2}. \tag{2.2.8}$$

This is proven in [25].

Now, we can use an O(4) symmetric polar-coordinate system and we can simplify the equation of motion to

$$\frac{d^2\phi}{d\rho^2} + \frac{3}{\rho}\frac{d\phi}{d\rho} - V'(\phi) = 0. \tag{2.2.9}$$

The Euclidean action of (2.2.1) takes the form

$$S_E(\phi) = 2\pi^2 \int_0^\infty d\rho\ \rho^3 \left[\frac{1}{2}\left(\frac{d\phi}{d\rho}\right)^2 + V(\phi)\right]. \tag{2.2.10}$$

The boundary conditions become also simpler with the (2.2.5) and (2.2.7) become a single condition

$$\phi(\rho \to \infty) \to \phi_{\text{fv}} \tag{2.2.11}$$

and ensure that the action of (2.2.10) converges. Furthermore, $\phi(\rho)$ should not be singular at the origin so

$$\dot{\phi}(0) = 0, \tag{2.2.12}$$

where dot indicates differentiation with respect to the radial parameter, ρ ($\dot{\phi} = \frac{d\phi}{d\rho}$).

Note that we can correspond the equation (2.2.9) with the motion of a particle rolling down an inverted potential, $-V(\phi)$, with ρ being the time and the second term behaving like a time dependent friction term. We understand from the

boundary conditions that the particle is released initially at rest. We also tune the position at time zero so as the particle will come to rest at $\phi_{\rm fv}$ at time infinity.

Evidently, there is no a unique solution to these equations as it is a two-point boundary value problem. For instance, one solution is $\phi_{\rm fv}$, the false vacuum solution and an other solution that do not satisfy the boundary conditions is $\phi_{\rm tv}$, with the ϕ being constant in the true vacuum. However, in flat space there is a unique non-trivial solution.

2.3 The Overshoot/Undershoot Method without Gravity

In this section, we will use the shooting method to solve (2.2.9) having in mind that the potential appears inverted since we did a Wick rotation. We should choose properly the initial field $\phi(0)$ so as to satisfy the (2.5.13). Noted that, if $\phi(0)$ is between the range ($\phi_{\rm fv}$, $\phi_{\rm tv}$), the solution will roll towards the top of the barrier, $\phi_{\rm bar}$, and will eventually cross it. Obviously, $\phi(0)$ has to be at the range ($\phi_{\rm bar}$, $\phi_{\rm tv}$) for satisfying the (2.5.13). The solutions, which start from $\phi_{\rm fv}$ or close to $\phi_{\rm fv}$, will fall back but they cannot reach $\phi_{\rm fv}$ due to the friction removing energy term.

Therefore, if $\phi(0)$ is between the range ($\phi_{\rm bar}$, $\phi_{\rm tv}$), there are two possibilities. The first possibility is the 'undershoot' solution: if $\phi(0)$ is too close to $\phi_{\rm bar}$, the solution will not have enough energy to climb to $\phi_{\rm fv}$ and it will oscillate forever around $\phi_{\rm bar}$ losing its energy. The contribution of this solution to the action is infinite. The other possibility is the 'overshoot' solution: if $\phi(0)$ is closer to $\phi_{\rm tv}$, the solution will overshoot and pass $\phi_{\rm fv}$ at some finite time. Then, the solution may oscillate about an other barrier, escape to infinity, or reflect backwards depending on the potential. Thus, we understand that by continuity, there must be an

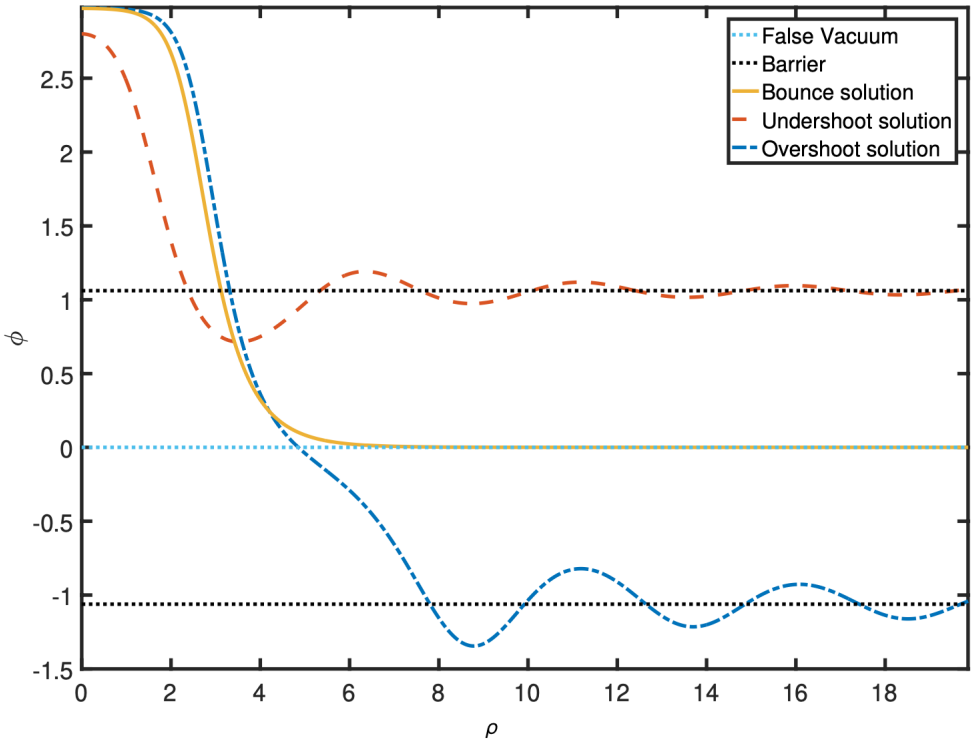

FIGURE 2.3.1: Overshoot, undershoot and bounce solutions of the equation (2.2.9). This is the case in which the overshoot solution oscillates about an other barrier.

intermediate initial position for which the solution comes to rest at ϕ_{fv}. This is the 'bounce' solution that dominates vacuum decay.

In order to determine this bounce solution, firstly, we determine one initial value $\phi(0)$ for an overshoot solution and one for an undershoot solution. Afterwards, using the method of bisection, we reduce the range between them and we know that the initial value $\phi(0)$ of the bounce solution is in this range. We repeat the same procedure so as to obtain more accurate bounce solution.

Overshoot, undershoot and bounce solutions are shown in figure 2.3.1. It is worth noting that the exact bounce solution cannot be determined numerically. We also note that these are the solutions of the equation (2.2.9) with a potential that has at least two minimums and two maximums since the overshoot solution starts near the true vacuum (first maximum) passes the barrier (first minimum)

and false vacuum (second maximum) and then oscillates about a second minimum. The undershoot solution oscillates about the barrier and the graph illustrates an undershoot solution that is not near the bounce solution. Obviously, we can find an undershoot solution closer to the bounce solution.

Uniqueness of Flat Space Bounces

Now, we will prove the aforementioned statement that there is a unique non-trivial solution in flat space using a single energy argument first given by Coleman [19]. Changing the form of the equation (2.2.9) to

$$\frac{d}{d\rho}\left(\frac{\dot{\phi}^2}{2} - V(\phi)\right) = -\frac{3}{\rho}\dot{\phi}^2 \ , \tag{2.3.1}$$

we notice that the friction term is always negative. Consequently, the energy of the system is monotonically decreasing. When we say the energy of the system, we mean the terms in the brackets of the left hand side of the equation (2.3.1). Although, this is different from the common definition of the energy as the potential has opposite sign due to Wick rotation, it does not affect our result, that is, the monotonically decreasing of the energy. For instance, when $\phi(0) = \phi_1$ and we have an undershoot solution as there is no enough energy to reach ϕ_{fv}, all solutions with $\phi(0)$ between the range (ϕ_{bar}, ϕ_1) will not have enough energy, and thus they will be undershoot solutions. A bounce solution always lies between a range of undershoots and a range of overshoots so we will not have a bounce solution with $\phi(0)$ closer to the barrier as it is always an undershoot solution. Therefore, we conclude that the bounce solution is unique because if there is a second solution, overshoot solutions are required on one side of it.

2.4 Thin-Wall Approximation

We can compute an approximate solution ϕ_{aprx} in the limit of small energy-density difference between the true and false vacuums [12, 19]. Let us consider a positive number

$$\epsilon = V(\phi_{\text{fv}}) - V(\phi_{\text{tv}}) \tag{2.4.1}$$

and a symmetric potential

$$V_0(\phi) = V_0(-\phi) \tag{2.4.2}$$

with two minimums at points $\pm a_0$. Therefore, in this case, we have

$$\phi_{\text{fv}} \approx -a_0, \tag{2.4.3}$$

$$\phi_{\text{tv}} \approx a_0 \tag{2.4.4}$$

to the lowest non-trivial order in ϵ. We can break the symmetry of the potential by adding to it a term proportional to ϵ

$$V = V_0 + \epsilon(a\phi + b) \ , \tag{2.4.5}$$

where a and b are constants. Obviously, if the ϵ term vanishes, we will not have vacuum decay due to degeneracy.

Now, we will show that we can calculate the decay exponent B of the equation (1.2.3) in closed form if we consider the thin-wall approximation.

From the mechanical side of view, we should choose the initial position of the particle $\phi(0)$ near the true vacuum and thus, the particle remains a lot of time there. In some large time $\rho = R$, the particle starts rolling down and then it goes to false vacuum and stays there forever. From the field-theoretic side of view, the solution looks like a large spherical four-dimensional bubble with a radius equal to R. Inside the bubble there is the true vacuum state and outside the false vacuum

state with a thin wall separating these two states. This wall has very small thick compared to the radius R and this is the reason why the approximation is called "thin-wall approximation".

We can discard the term which is proportional to ϵ in

$$\ddot{\phi} + \frac{3}{\rho}\dot{\phi} - V'(\phi) = 0, \tag{2.4.6}$$

since we are in the limit of small energy-density difference between the vacuums. When $\rho \approx R$, we can neglect the term which is proportional to $\dot{\phi}$ as we are in the limit of large $\rho = R$. Away from the wall, $\dot{\phi}$ is also negligible. Therefore, the approximate ϕ obeys the equation

$$\frac{d^2\phi}{dx^2} = V_0'(\phi) \ , \tag{2.4.7}$$

where x is the spatial variable in one-dimensional theory.

Now, we can solve the equation (2.4.7) analytically. First, we integrate it

$$\frac{1}{2}\left(\frac{d\phi}{dx}\right)^2 = V_0(\phi) + c, \tag{2.4.8}$$

where c is a constant that can be specified by the condition $\phi(\infty) = \phi_{\rm fv}$. The approximate solution $\phi_{\rm aprx}$ is defined by

$$x - R = \int_{[\phi_{\rm tv}+\phi_{\rm fv}]/2=0}^{\phi_{\rm aprx}} \frac{d\phi}{[2(V_0(\phi) - V_0(\phi_{\rm fv}))]^{\frac{1}{2}}}, \tag{2.4.9}$$

where we choose R to be the point at which the field ϕ is the average of its two extreme values. Evidently, the form of the action of this solution is

$$\begin{aligned} S_{\rm aprx} &= \int dx \left[\frac{1}{2}\left(\frac{d\phi}{dx}\right)^2 + V_0(\phi) - V_0(\phi_{\rm fv})\right] \\ &= \int_{-a_0}^{a_0} d\phi \ \left[2(V_0(\phi) - V_0(\phi_{\rm fv})\right]^{\frac{1}{2}}. \end{aligned} \tag{2.4.10}$$

Now, we will compute the only thing missing from this description, the value of radius R, by calculating the value of coefficient B in closed form. The four-dimensional action is

$$S_E(\phi) = 2\pi^2 \int_0^\infty d\rho\ \rho^3 \left[\frac{1}{2}\left(\frac{d\phi}{d\rho}\right)^2 + V(\phi)\right]. \tag{2.4.11}$$

At first, we should realize that this coefficient is divided into three parts: outside the wall, inside the wall and the wall itself. As we know, outside the wall ($\rho \in (R, \infty)$) $\phi = \phi_{\text{fv}}$ so

$$B_{\text{outside}} = 0, \tag{2.4.12}$$

inside the wall ($\rho \in (0, R)$) $\phi = \phi_{\text{tv}}$ and thus:

$$B_{\text{inside}} = -\frac{1}{2}\pi^2 R^4 \epsilon. \tag{2.4.13}$$

Within the wall, the coefficient is

$$B_{\text{wall}} = 2\pi^2 R^3 \int d\rho \left[\frac{1}{2}\left(\frac{d\phi}{d\rho}\right)^2 + V_0(\phi) - V_0(\phi_{\text{fv}})\right] \tag{2.4.14}$$

$$= 2\pi^2 R^3 S_{\text{aprx}}. \tag{2.4.15}$$

The total B is

$$B = -\frac{1}{2}\pi^2 R^4 \epsilon + 2\pi^2 R^3 S_{\text{aprx}}. \tag{2.4.16}$$

Note that, we can determine the value of R by finding the point that the coefficient B is stationary

$$\frac{dB}{dR} = -2\pi^2 R^3 \epsilon + 6\pi^2 R^2 S_{\text{aprx}} = 0. \tag{2.4.17}$$

Hence,

$$R = 3S_{\text{aprx}}/\epsilon, \tag{2.4.18}$$

and this can justify our approximation since when ϵ becomes small, R becomes

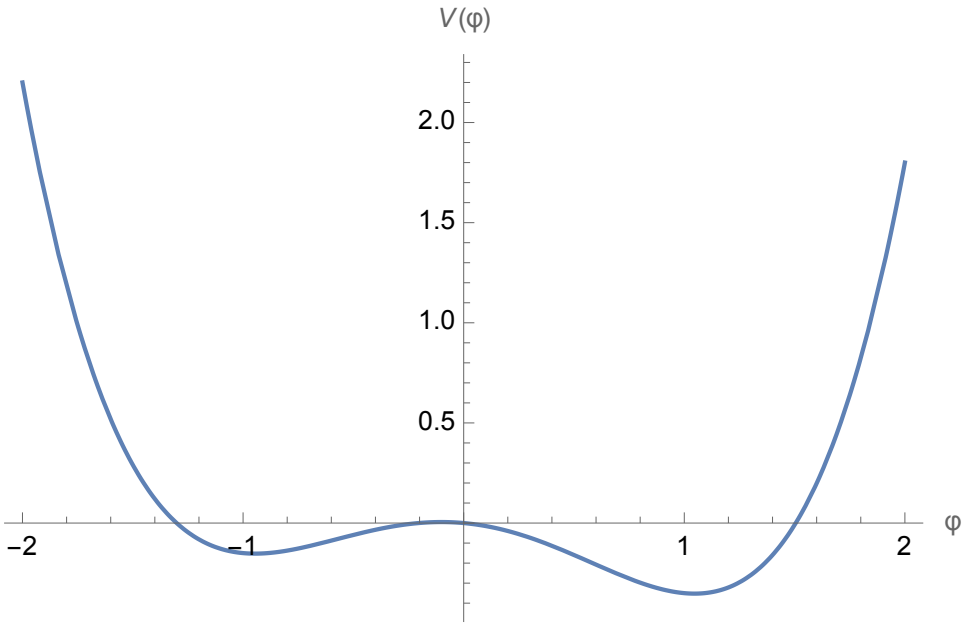

FIGURE 2.5.1: Simple polynomial potential of the equation (2.5.1)

large. By determining the value of R, we can obtain the desired closed-form expression for the coefficient B in this approximation

$$B = 27\pi^2 S_{\text{aprx}}^4 / 2\epsilon^3. \tag{2.4.19}$$

From this expression, we can compute now the probability of the false vacuum decay.

2.5 Application to a Polynomial Potential

In this section, we apply some notions that we discussed in the previous sections and we present numerical calculations of the bounce solutions. We firstly consider a simple polynomial potential

$$V(\phi) = -\frac{1}{2}\phi^2 + \frac{1}{4}\phi^4 - 0.1\phi \tag{2.5.1}$$

that is demonstrated in figure 2.5.1.

Afterwards, we determine the exact values of true and false vacuum by finding the points of the two minimums of the potential. The true and the false vacuums are at

$$\phi_{\text{tv}} = 1.04668053 \tag{2.5.2}$$

and

$$\phi_{\text{fv}} = -0.94564927, \tag{2.5.3}$$

respectively. In this case, the equation of motion of (2.2.9) takes the form

$$\frac{d^2\phi}{d\rho^2} + \frac{3}{\rho}\frac{d\phi}{d\rho} = -\phi + \phi^3 - 0.1 \ . \tag{2.5.4}$$

Now, using the overshoot/undershoot method, we try to find the initial condition $\phi(0)$ of the solution having in mind that $\dot{\phi}(0) = 0$. Specifically, the bounce solution can be computed by means of a binary search on the boundaries between overshoot and undershoot regions as it was described in section (2.2). Hence, we determine that

$$\phi_{\text{undershoot}}(0) = 1.046680379, \tag{2.5.5}$$

$$\phi_{\text{overshoot}}(0) = 1.046680380 \tag{2.5.6}$$

and thus, the $\phi(0)$ for the exact solution is between these two values. We can see the undershoot and overshoot solutions for this example in figure 2.5.2. We notice that the undershoot solution oscillates around the top barrier and the overshoot solution goes over the false vacuum and to infinity. Of course, using this approach we never find a solution that actually satisfy the boundary condition of the equation (2.5.13), and instead, we try to find a solution that stays close to the false vacuum as long as possible. We consider that the bounce solution is the same to overshoot and undershoot solutions up to the point that these two solutions become different. Obviously, in this case, this point is $\rho = 18$.

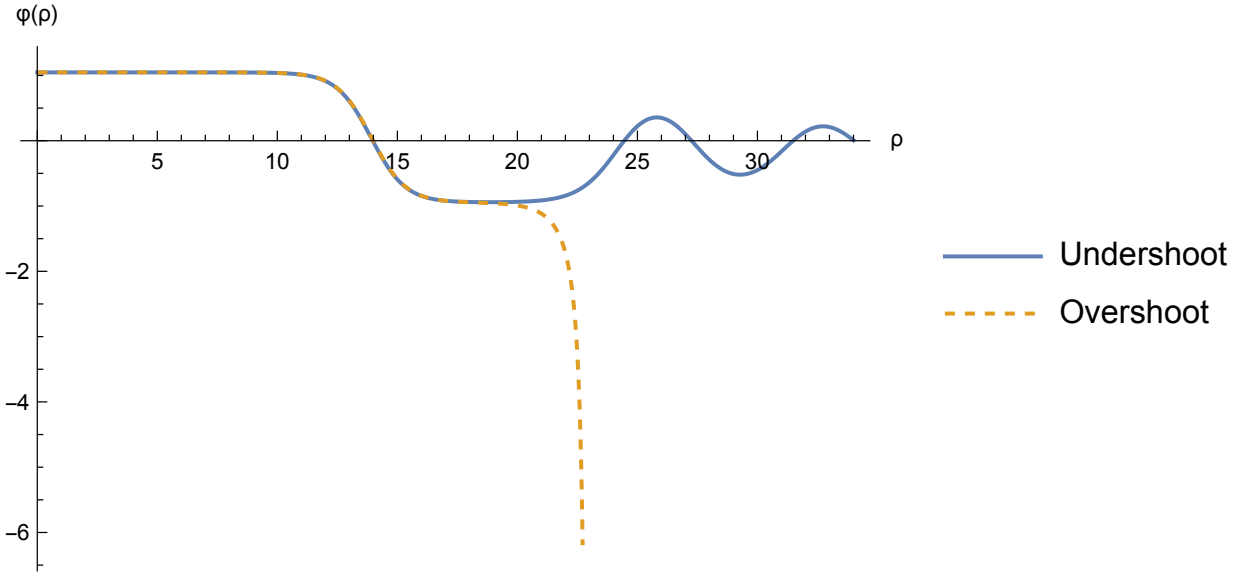

FIGURE 2.5.2: The undershoot and overshoot solutions for the potential of the equation (2.5.1)

Finally, we calculate the decay exponent B for the undershoot and overshoot solution. This exponent will help us to compute the probability of the false vacuum decay. We apply this example to equations (1.2.10) and (2.2.10) having in mind that we should integrate up to $\rho = 18$ and we determine the values of coefficient B as

$$B_{\text{undershoot}} = 12358.1, \tag{2.5.7}$$

$$B_{\text{overshoot}} = 12359.2\ . \tag{2.5.8}$$

It is worth mentioning that these two results are the same up to a numerical error.

Thin-Wall Approximation

Now, we use the thin-wall approximation in order to verify our previous solution. As we mentioned, we can find our solution analytically in this approximation. The first thing that we should do is to determine the parameter ϵ of the equation (2.4.1) for this simple polynomial potential

$$\epsilon = 0.199747. \tag{2.5.9}$$

As we discussed in the previous section, we neglect some terms in equation (2.5.4) and now our approximate equation of motion is

$$\frac{d^2\phi}{d\rho^2} = -\phi + \phi^3, \tag{2.5.10}$$

like the equation (2.4.7). Note that, the symmetric potential is a double well potential

$$V_0(\phi) = -\frac{1}{2}\phi^2 + \frac{1}{4}\phi^4, \tag{2.5.11}$$

with two minimums at $\phi = \pm 1$. Then, we integrate the equation (2.5.10) and we end up with the following equation

$$\frac{1}{2}\left(\frac{d\phi}{d\rho}\right)^2 = -\frac{1}{2}\phi^2 + \frac{1}{4}\phi^4 + \frac{1}{4}\ , \tag{2.5.12}$$

with the constant of integration equal to $1/4$ due to the boundary condition

$$\phi(\rho \to \infty) \to \phi_{\text{fv}}. \tag{2.5.13}$$

When we manipulate this equation, it takes this form

$$\rho - R = -\int_0^{\phi_{\text{aprx}}} \frac{\sqrt{2}\ d\phi}{1-\phi^2}. \tag{2.5.14}$$

Writing the solution as an integral of an odd function is the real benefit of the thin-wall approximation. For this specific potential, we can solve analytically this integration

$$\rho - R = -\sqrt{2}\ \text{arctanh}(\phi_{\text{aprx}}). \tag{2.5.15}$$

Hence, we get the solution of the thin wall approximation

$$\phi_{\text{aprx}}(\rho) = -\tanh\left(\frac{\rho - R}{\sqrt{2}}\right). \tag{2.5.16}$$

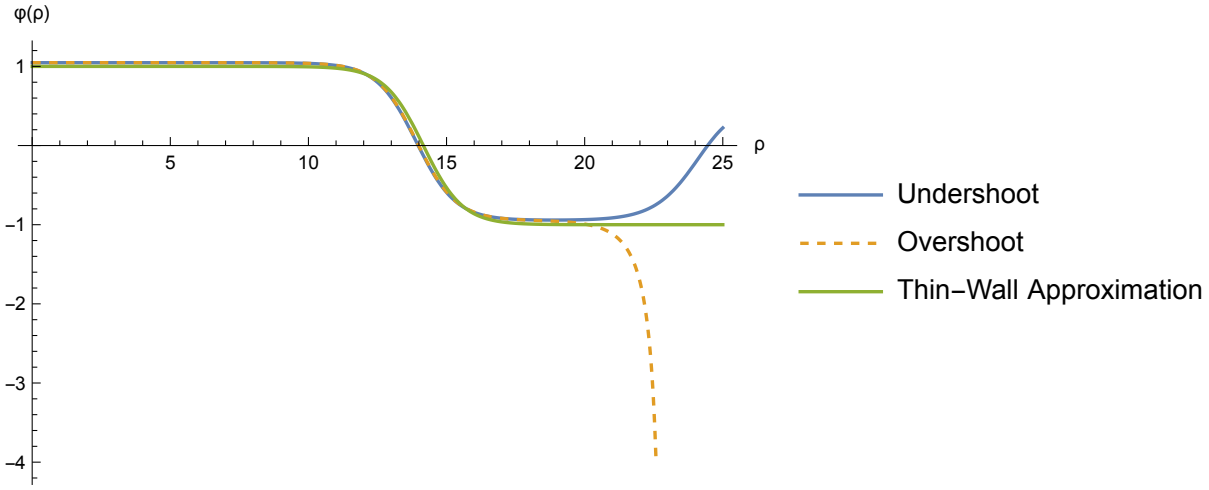

FIGURE 2.5.3: The thin-wall solution compared with the undershoot and overshoot solutions

We can also determine the value of R numerically from equation (2.4.18)

$$R = 14.160066830, \tag{2.5.17}$$

and thus,

$$\phi_{\text{aprx}}(\rho) = -\tanh\left(\frac{\rho - 14.160066830}{\sqrt{2}}\right). \tag{2.5.18}$$

The approximate solution is shown in figure (2.5.3) where we can compare it with undershoot and overshoot solutions.

By calculating the action S_{aprx} of this approximate solution

$$S_{\text{aprx}} = \int_{-1}^{1} d\phi \left[\frac{1}{2}(1-\phi^2)\right], \tag{2.5.19}$$

and by using the equation of the closed-form expression for the coefficient B

$$B = 27\pi^2 S_{\text{aprx}}^4 / 2\epsilon^3, \tag{2.5.20}$$

we can find the numerical value of the decay exponent B

$$B_{\text{approximate}} = 13209.6\ . \tag{2.5.21}$$

We notice that it is almost the same to the overshoot and undershoot decay exponent and thus, we verify our solution. The difference between the three decay exponents is due to numerical errors.

Chapter 3

Vacuum Decay in Curved Spacetime

3.1 Barrier Penetration in Field Theory with Gravity

In this section, we extent the theory of the previous chapter to a theory of a scalar field interacting with gravity. Many authors conducted research on this topic, especially how gravity affects vacuum bubbles [13, 26, 27, 28, 29, 30].

The expression for the probability of decay of the false vacuum per unit time per unit volume in this theory is the same as before i.e. the same to the equation (1.2.3). However, for computing the coefficients A and B, we consider the following Euclidean action [31]

$$S_E[\phi, g_{\mu\nu}] = \int d^4x \sqrt{|\det g|} \left[\frac{1}{2} \nabla_\mu \phi \nabla^\mu \phi + V(\phi) - \frac{M_p^2}{2} R \right], \tag{3.1.1}$$

where M_p is the "reduced Planck mass", $M_p = \frac{1}{\sqrt{8\pi G_N}}$, and R is the Ricci scalar. Specifically, coefficient A can be determined by calculating functional determinant fluctuations around a bounce solution of this action. This prefactor A is known in the flat-space case [32], but has yet to be computed in a curved background.

The decay exponent B is the difference of the action of a bounce solution and the action of the "false-vacuum solution"

$$B = S[\phi, g_{\mu\nu}] - S[\phi_{\rm fv}, g_{{\rm fv}\mu\nu}]. \tag{3.1.2}$$

The "false-vacuum solution" is a solution where the field is always constant and it is equal to the false vacuum state. As before, the bounce solution is the solution that contributes to the decay since it has the smallest action and thus, the smallest decay exponent B. In order to find the bounce solution, we need to solve the Euclidean equations of motion obeying appropriate boundary conditions.

In the action of the equation (3.1.1), we can add a cosmological constant but here we absorb this constant in the potential $V(\phi)$. We also neglect boundary terms since we can add a Gibbons-Hawking-York term to the action [33]. It is worth mentioning that these boundary terms do not contribute to the decay rate as the two solutions are identical on the boundary of the Euclidean spacetime [34].

The aforementioned Euclidean equations of motion of the action (3.1.1) that should be solved are

$$\nabla_\mu \nabla^\mu \phi - V'(\phi) = 0, \tag{3.1.3}$$

$$R_{\mu\nu} - \frac{1}{2} R g_{\mu\nu} = \frac{1}{M_P^2}\left(\nabla_\mu\phi\nabla_\nu\phi - \frac{1}{2} g_{\mu\nu}\left[\frac{1}{2}\nabla_\rho\phi\nabla^\rho\phi + 2V(\phi)\right]\right). \tag{3.1.4}$$

At this point, we assume that the bounce is invariant under four-dimensional rotations so as to simplify these equations. We can assume this O(4) rotational symmetry as there is no reason for gravitation to break the symmetries of the theory in the absence of gravity [35, 36]. Under this assumption, the form of the Euclidean metric is

$$ds_E^2 = d\rho^2 + a(\rho)^2 d\Omega_3^2 \ , \tag{3.1.5}$$

where $d\Omega_3^2$ is the unit of three-sphere metric, ρ is the radial coordinate and $a(\rho)$ gives the radius of curvature of each three-sphere of coordinate radius ρ. It is worth mentioning that by assuming O(4) symmetry, we reduce our ten unknown functions of four variables to one unknown function of one variable. We also reduce the equations of motion to

$$\ddot{\phi} + \frac{3\dot{a}}{a}\dot{\phi} - V'(\phi) = 0, \tag{3.1.6}$$

$$\dot{a}^2 = 1 - \frac{a^2}{3M_P^2}\left(- \frac{\dot{\phi}^2}{2} + V(\phi)\right), \tag{3.1.7}$$

$$\ddot{a} = -\frac{a}{3M_P^2}\left(\dot{\phi}^2 + V(\phi)\right), \tag{3.1.8}$$

where dots represent differentiation with respect to the radial coordinate ρ. Evidently, when you differentiate the equation (3.1.7), which is similar to Friedmann equation of cosmology but with different interpretation, the result is the equation (3.1.8). The latter is preferable as we do not need to choose the sign of the equation and thus, it is easier to use it numerically. Not choosing the sign is important since a changes continuously sign in de Sitter space.

As we assume O(4) symmetry, the surfaces of constant ρ have always positive curvature and of course, they are three-dimensional spheres. Therefore, the first term of the equation (3.1.7) is always one and the "spatial" curvature is always positive. However, the full four-dimensional curvature can be either positive or negative. The form of the Ricci scalar is

$$R = \frac{\dot{\phi}^2 + 4V(\phi)}{M_P^2} = \frac{6(1-\dot{a}^2)}{a^2} - \frac{6\ddot{a}}{a}. \tag{3.1.9}$$

We notice here that the curvature can be negative when the potential becomes negative. This can happen in the interior of the bubble where the true vacuum state is.

Additionally, for these equations of motion, after some manipulation, the action is given by

$$S[\phi, a] = -2\pi^2 \int_0^{\rho_{\max}} d\rho \; a^3(\rho) V(\phi(\rho)), \tag{3.1.10}$$

and thus, the decay exponent B is

$$B = \frac{24\pi^2 M_P^4}{V_0} - 2\pi^2 \int_0^{\rho_{\max}} d\rho \; a^3(\rho) V(\phi(\rho)) \; , \tag{3.1.11}$$

where $V_0 = V(\phi_{\text{fv}})$ is the value of the potential in the false vacuum state and $\rho_{\max}$ is the maximum value that the radial coordinate can be in this coordinate system. It may be either finite or infinite.

Boundary Conditions

Now, we impose boundary conditions in order to be sure that the decay exponent B is finite. At first, we impose $a(0) = 0$ so as to define that $\rho = 0$ is at the centre of the bounce. Specifically, we know that a describes the radius of the curvature of a surface with a specific ρ and the surface at $\rho = 0$ is a single point. In addition, we desire smoothness of the solution at the $a(0) = 0$ coordinate singularity so we imply $\dot{\phi}(0) = 0$ like in the flat space. Finally, we require a second boundary condition for the field ϕ so as our problem is fully specified.

For this boundary condition, there are two cases depending on the sign of the potential in the false vacuum, $V(\phi_{\text{fv}})$. In the first case, when $V(\phi_{\text{fv}})$ is positive and the solution is compact, there is a finite point $\rho_{\max} > 0$ where $a(\rho_{\max}) = 0$. Therefore, we impose

$$\dot{\phi}(\rho_{\max}) = 0, \tag{3.1.12}$$

since we also want a smooth solution at this second coordinate singularity. Note that, this compact manifold is a three-sphere where $\rho = 0$ can be the north pole and $\rho = \rho_{\max}$ can be the south pole. In the second case, when $V(\phi_{\text{fv}})$ is negative

or equal to zero, the the solution is non-compact and we require

$$\phi(\rho \to \infty) \to \phi_{\text{fv}}, \tag{3.1.13}$$

in order to have a finite decay exponent B. Imposing this boundary condition, we require $a^3(\rho)V(\phi(\rho))$ to approach zero sufficiently fast since $a(\rho \to \infty)$ is non-zero so as to have a finite decay exponent B.

3.2 Types of Gravitational Solutions

Flat False Vacuum Bounce

When the potential in the false vacuum is equal to zero, $V(\phi_{\text{fv}}) = 0$, we have a non-compact solution, the flat false vacuum bounce. As we mentioned in the previous section, this is the case in which the boundary conditions are $\dot{\phi}(0) = 0$ and $\phi(\rho \to \infty) \to \phi_{\text{fv}}$. Therefore, this solution is quite similar to the solution in the absence of gravity as they have similar properties.

We notice that at large ρ, the field approaches the false vacuum state and thus, $a(\rho) \to \rho$ which transforms the metric to the flat space metric. This happens outside of the bounce. Hence, the gravity is restricted inside the bounce where the scalar field is the deepest so we expect more significant gravitational corrections. Inside the bounce, the space is an anti-de Sitter space with a negative Ricci scalar as the potential is less than zero. For this reason, there is a possibility for a bubble to experience a gravitational collapse.

Hawking-Moss Bounce

Hawking-Moss solution is a simple solution which is constant at the top of the barrier [37]

$$\phi(\rho) = \phi_{\text{HM}}. \tag{3.2.1}$$

Solving the equation (3.1.7), we find

$$a(\rho) = \frac{1}{H_{\rm HM}} \sin\big(H_{\rm HM}\rho\big), \tag{3.2.2}$$

where $H^2_{\rm HM} = \frac{V(\phi_{\rm HM})}{3M_P^2}$. The decay exponent B for this solution is trivial

$$B = S[\phi_{HM}] - S[\phi_{\rm fv}] = 24\pi^2 M_P^4 \bigg(\frac{1}{V_0} - \frac{1}{V(\phi_{\rm HM})}\bigg). \tag{3.2.3}$$

Now, when $\Delta V(\phi_{\rm HM}) = |V(\phi_{\rm HM}) - V_0| << |V_0|$, we can compute an approximate B

$$B \approx \frac{8\pi^2 \Delta V(\phi_{\rm HM})}{3H^4_{\rm HM}}. \tag{3.2.4}$$

We observe that this is the ratio of the energy that is required to excite a sphere with Hubble volume (a volume with radius $\frac{1}{H_{\rm HM}}$) to the top of the barrier over the Gibbons-Hawking temperature $\frac{H_{\rm HM}}{2\pi}$. Therefore, the Hawking-Moss solution can be explained by a thermal interpretation and it has a completely thermal character [38].

Coleman-de Luccia Bounce

Now, when $V(\phi_{\rm fv}) > 0$, there may or may not exist a non-trivial solution that satisfies the boundary conditions $\dot{\phi}(0) = 0$ and $\dot{\phi}(\rho_{\rm max}) = 0$. The existence of this solution depends on the form of the potential and it is called Coleman-de Luccia solution [12]. We define that this non-trivial bounce crosses the barrier only once. CdL solution only satisfies $\dot{\phi} = 0$ at the boundaries and nowhere else and thus it is a monotonic bounce between $\phi(0)$ and $\phi(\rho_{\rm max})$. It is worth mentioning that according to Weinberg and Hackworth [39], some shapes of potential can lead to multiple CdL bounces crossing the barrier only once.

Oscillating Bounce

There is also a bounce that satisfies the same boundary conditions as a CdL solution ($\dot{\phi}(0) = 0$ and $\dot{\phi}(\rho_{\rm max}) = 0$) but this bounce crosses the barrier more than

once. This solution is called the Oscillating bounce and it is not monotonic in the range $(0, \rho_{\max})$ i.e. there are additional turning points between the aforementioned interval.

At first glimpse, it seems that such solution contribute to the probability of the decay rate. However, Oscillating bounce has more than one negative eigenvalue in the space of linear fluctuations so it does not contribute to the vacuum decay [40, 41, 42]. Note that, the number that bounce crosses the barrier is the number of the negative modes of the bounce. Otherwise, CdL solution has only one negative mode and it can contribute to the decay rate.

3.3 The Critical Threshold and the Existence of Bounce Solutions

In this section, we present the critical Hubble rate and we discuss when each type of solution starts existing. At first, we define the background Hubble rate as

$$H^2 = \frac{V_0}{3M_P^2} \tag{3.3.1}$$

and the critical background Hubble rate as

$$H^2_{\text{crit}} = \frac{V_{0\text{crit}}}{3M_P^2} = -\frac{V''(\phi_{\text{HM}})}{4} - \frac{[V(\phi_{\text{HM}}) - V_0]}{3M_P^2}, \tag{3.3.2}$$

where ϕ_{HM} is the Hawking-Moss solution. The critical Hubble rate is very important in the subject of vacuum decay in de Sitter space since below of it, the Hawking-Moss solution starts having additional negative modes so it stops contributing to the tunneling process [38, 43]. As we mentioned before, when we have more than one negative mode there is always a bounce with lower action which contribute to vacuum decay.

Therefore, when $H < H_{\rm crit}$, CdL solutions always exist and dominate the decay rate of a false vacuum. However, when $H > H_{\rm crit}$, CdL solutions may or may not exist and this depends on the form of the potential. For instance, in the potential of Standard Model, there are CdL solutions above the critical threshold. If there are not any CdL solutions when $H > H_{\rm crit}$, the Hawking-Moss solution controls quantum tunneling. In this case, by continuity, we conclude that the CdL solution should tend to the Hawking-Moss solution when the Hubble rate H approaches its critical value. In the other case, where CdL solutions exist when $H > H_{\rm crit}$, we know that CdL solutions must me more than one [31].

According to [31] and [44], there is a quantity Δ that can determine if there are CdL solutions when $H > H_{\rm crit}$. This quantity has the following form

$$\Delta = -\frac{(\phi(0) - \phi_{\rm HM})^2}{14H^2}\left[V^{(4)}(\phi_{\rm HM}) + \frac{V^{(3)}(\phi_{\rm HM})^2}{12H^2}\right], \tag{3.3.3}$$

where $V^{(4)}(\phi_{\rm HM})$ and $V^{(3)}(\phi_{\rm HM})$ are the third and fourth derivatives of the potential at the top of the barrier. If this quantity is positive, CdL solutions exist for $H > H_{\rm crit}$. For instance, this is the case for the Standard Model potential.

3.4 The Overshoot/Undershoot Method with Gravity

In this section, we discuss the shooting method with gravity which is a bit trickier than the shooting method without gravity. The main difference is that in curved space, the friction term can also be negative and it is transformed to an anti-friction term that gives energy to the system. This is the case when $\dot{a} < 0$ in the following equation

$$\frac{d}{d\rho}\left(\frac{\dot{\phi}^2}{2} - V(\phi)\right) = -\frac{3\dot{a}}{a}\dot{\phi}^2. \tag{3.4.1}$$

Therefore, the statement that if $\phi(0)$ is near the top of the barrier, we will have an undershoot solution, is not valid anymore.

In general, it is common that when you choose a specific $\phi(0)$, you have a solution of equations of motion that does not satisfy the bounce boundary conditions. Therefore, we tune the initial value $\phi(0)$ to find undershoot and overshoot solutions in the same way as in the section (2.3).

In the presence of gravity, overshoot and undershoot solutions have different notion. The former is a noninstanton solution that diverges on the opposite side of the barrier to that on which they start and the latter diverges on the same side of the barrier. An easier way to consider overshoot and undershoot solutions is to define them by the number of times N that they cross the barrier. Balek and Demetrian argue that if we have two noninstanton solutions and one of them crosses the barrier one more time than the other (N+1), continuity demands a bounce solution between them which crosses the top of the barrier N times [45]. Therefore, we can find bounce solutions by the method of bisection.

As we are only interested in CdL solutions since they contribute to the vacuum decay, we concentrate only to solutions that cross the barrier once or twice because CdL solution crosses the barrier once. In this case, we define the overshoot solution as a noninstanton solution that does not undergo $\dot{\phi} = 0$ before the second coordinate singularity, where $a = 0$, i.e. its derivative $\dot{\phi}$ has no nodes since it is a monotonic solution. We also define the undershoot solution as a noninstanton solution that has derivative $\dot{\phi}$ with one node.

Chapter 4

Vacuum Decay with Fixed De Sitter Background

4.1 Barrier Penetration in Field Theory with Fixed De Sitter Background

In this chapter, we discuss the notions of the previous chapter but now with a fixed de Sitter background. Obviously, the calculation of solutions in a fixed background is simpler as we assume that the background is unaffected by back-reaction of the bounce solution.

We use the fixed background approximation by assuming that the function of $a(\rho)$ takes the same form of $a(\rho)$ of the false-vacuum solution

$$a(\rho) = \frac{1}{H_0}\sin(H_0\rho), \tag{4.1.1}$$

where

$$H_0^2 = \frac{V_0}{3M_P^2}, \tag{4.1.2}$$

where again $V_0 = V(\phi_{\rm fv})$. In this way, we manage to ignore the effects of back-reaction from the bounce solution on the metric.

The form of the Euclidean action is the same as the equation (3.1.1), but now the Ricci scalar R has a constant value. Therefore, we can ignore it as we are interested only in the difference of two actions in order to calculate the decay exponent B by considering the equation (3.1.2).

Now, we have only one differential equation

$$\nabla_\mu \nabla^\mu \phi - V'(\phi) = 0, \tag{4.1.3}$$

and by assuming O(4) rotational symmetry, this equation takes the following form

$$\ddot{\phi} + \frac{3\dot{a}}{a}\dot{\phi} - V'(\phi) = 0. \tag{4.1.4}$$

Substituting (4.1.1) in the action and assuming O(4) symmetry, we get the following simple form of the action

$$S[\phi, a] = 2\pi^2 \int_0^{\rho_{\rm max}} d\rho \, \frac{\sin^3(H_0\rho)}{H_0^3}\left(\frac{\dot{\phi}^2}{2} + V(\phi(\rho))\right), \tag{4.1.5}$$

where now the radial coordinate $\rho_{\rm max}$ is finite as we consider non-zero, positive V_0 and thus we have compact solutions. The value of $\rho_{\rm max}$ is equal to

$$\rho_{\rm max} = \frac{\pi}{H_0}, \tag{4.1.6}$$

since in this point we have coordinate singularity ($a(\frac{\pi}{H_0}) = 0$) for the first time after $a(0) = 0$. Hence, the decay exponent B is

$$B = 2\pi^2 \int_0^{\frac{\pi}{H_0}} d\rho \, \frac{\sin^3(H_0\rho)}{H_0^3}\left(\frac{\dot{\phi}^2}{2} + V(\phi(\rho))\right) - \frac{24\pi^2 M_P^4}{V_0}. \tag{4.1.7}$$

As our solution is compact, the boundary conditions for ϕ are

$$\dot{\phi}(0) = 0, \tag{4.1.8}$$

$$\dot{\phi}\left(\frac{\pi}{H_0}\right) = 0. \tag{4.1.9}$$

However, we use shooting method and we tune the initial value $\phi(0)$ in order to get overshoot and undershoot solutions as we mentioned in the previous chapter.

In this case, the expression of the decay exponent B of the Hawking-Moss solution is different from the general case in which $a(\rho)$ is dynamical. As we know, Hawking-Moss solution is a constant solution at the top of the barrier. Now, instead of considering this equation (3.2.2), we assume this equation (4.1.1) as we demand a fixed de Sitter background. Consequently, according to the equation (4.1.7), the decay exponent B of the Hawking-Moss solution with a fixed background takes the form

$$B = 24\pi^2 M_P^4 \left(\frac{V(\phi_{\rm HM}) - V_0}{V_0^2}\right). \tag{4.1.10}$$

An other notion that is slightly different in the case of the fixed background approximation is the critical Hubble rate. Now, it has the following form [31]

$$H_{\rm crit}^2 = \frac{V_{0\rm crit}}{3M_P^2} = -\frac{V''(\phi_{\rm HM})}{4}, \tag{4.1.11}$$

where $\phi_{\rm HM}$ is the Hawking-Moss solution.

4.2 Application to a Polynomial Potential

The aim of this section is to apply the notions of the previous section to a polynomial potential so as to present the bounce solutions and the decay exponents B in

a fixed de Sitter background. We study the following simple polynomial potential

$$V(\phi) = -\frac{1}{2}\phi^2 + \frac{1}{4}\phi^4 - 0.1\phi + V_1, \tag{4.2.1}$$

where V_1 is a constant term. The true and the false vacuums as well as the position of the top of the barrier are the same as in section (2.5) since the only difference between the two potentials is a constant term. Note that

$$V_1 > 0.152639 \tag{4.2.2}$$

in order for the false-vacuum potential to be a non-zero, positive potential. Therefore, we have a compact space and CdL solutions. We also note that in this section, we work in units that $M_P = 1$.

Using the equation (4.1.11), we can determine the value of H_{crit} in this simple potential

$$H_{\text{crit}} = 0.492285. \tag{4.2.3}$$

Therefore, we can calculate the value of $V_{0\text{crit}}$

$$V_{0\text{crit}} = 0.727034 \tag{4.2.4}$$

for the false-vacuum potential. When we apply this potential to the quantity Δ in equation (3.3.3), we notice that this quantity is negative so we conclude that CdL solutions do not exist for $H > H_{\text{crit}}$.

Following the shooting method that was discussed in previous sections, we determine the CdL solutions for various values of V_0 of the polynomial potential (4.2.1). Specifically, the constant term V_1 is varied so as to get different values of false-vacuum potential V_0. These solutions are presented in figure 4.2.1. From the aforementioned figure, we observe that as $V_0 \to V_{0\text{crit}}$ from bellow, the amplitude

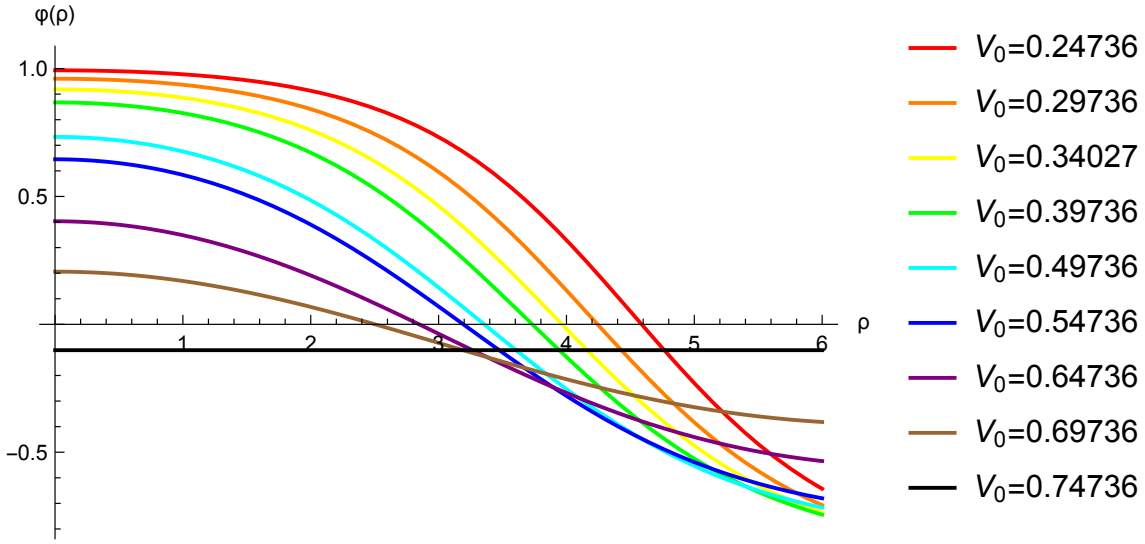

FIGURE 4.2.1: CdL solutions for various values of V_0 of the polynomial potential (4.2.1) in a fixed background

of the solution decreases and reaches zero as V_0 is raised past the critical value. In other words, in the limit of $V_0 \to V_{0\text{crit}}$ from bellow, CdL solution approaches smoothly the constant Hawking-Moss solution. On the flip side, in the limit of $V_0 \to 0$ ($V_1 \to 0.152639$), the amplitude of CdL solution increases and approaches the flat-space solution. This phenomenon is apparent in figure 4.2.2. Although, we know that the CdL solution of $V_0 = 0$ should be exactly the same as the flat-space solution, we can notice from figure 4.2.2 that they start deviating from each other when we go to higher ρ. Evidently, the numerical effects cause this deviation since we use different set of equations to determine these two solutions.

It is worth mentioning that each CdL solution with a positive value of $\phi(0)$ corresponds to a CdL solution with a negative initial value. These two solutions have the same value of decay exponent B and they are considered as the same solution. This has to do with a symmetry in our compact manifold, the symmetry between the south and the north pole of the sphere.

In addition, the decay exponents B for various values of V_0 are computed and illustrated in two graphs. The first graph 4.2.3 shows the relation between the decay exponent B and the false-vacuum potential V_0. The second graph 4.2.4

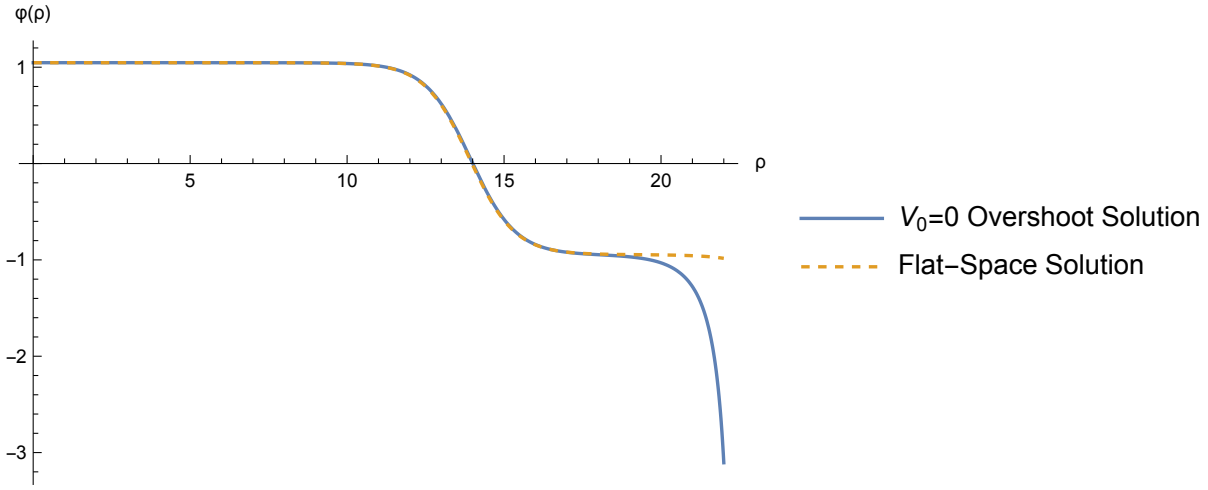

FIGURE 4.2.2: CdL solution in the limit of $V_0 \to 0$ ($V_1 \to 0.152639$) compared to the flat-space solution of the same potential

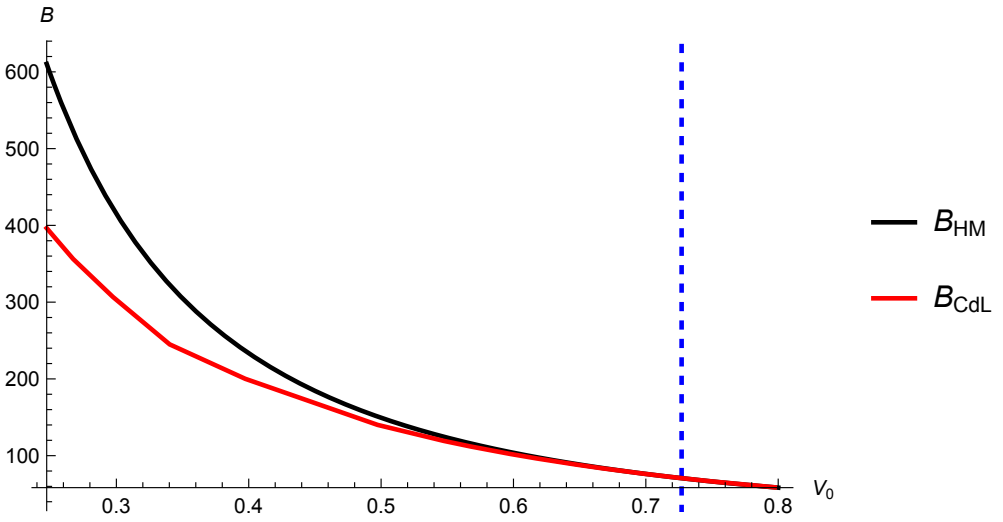

FIGURE 4.2.3: Decay exponent B vs false-vacuum potential V_0 graph in a fixed background. The dashed blue vertical line indicates the position of $V_{0\text{crit}}$.

demonstrates the difference between the decay exponent of Hawking-Moss solution and CdL solution for a given false-vacuum potential V_0. The dashed blue vertical line indicates the position of $V_{0\text{crit}}$.

Approaching the critical threshold, we notice that the decay exponent B of CdL solution merges with the decay exponent B of Hawking-Moss solution. From figure 4.2.4, we can verify the previous state as we observe that when $V_0 \to V_{0\text{crit}}$, the difference of the two exponents smoothly tends to zero. The reason for this

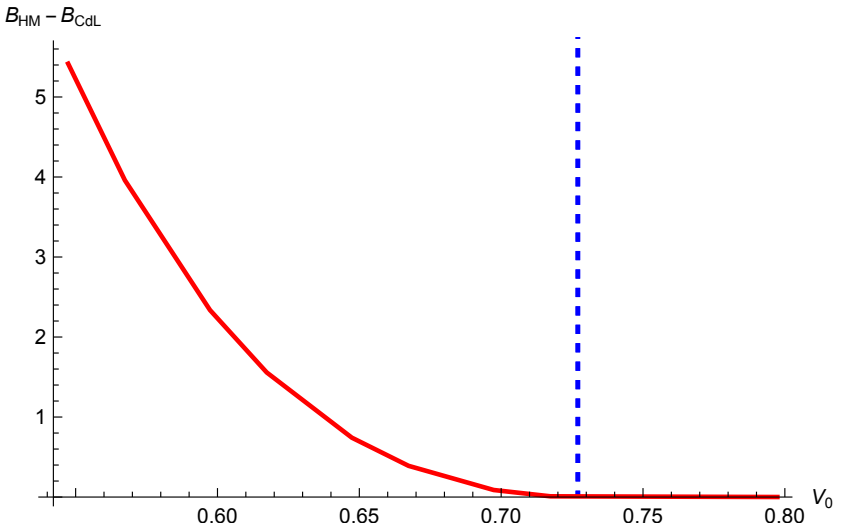

FIGURE 4.2.4: Difference between the decay exponent of Hawking-Moss solution and CdL solution vs false-vacuum potential V_0 graph in a fixed background. The dashed blue vertical line indicates the position of $V_{0\text{crit}}$.

is the fact that no CdL solution exists and the Hawking-Moss solution dominates above $V_{0\text{crit}}$.

In this section, we verify the idea that bellow H_{crit}, CdL solutions dominate and as we reach the critical threshold, CdL solutions smoothly merge the Hawking-Moss solution until they stop existing at H_{crit}. Consequently, above H_{crit}, Hawking-Moss solution dominates. We call this phenomenon the CdL-Hawking-Moss transition and as we mentioned again this is not a universal phenomenon.

Chapter 5

Vacuum Decay with Dynamical Gravity

5.1 The Overshoot/Undershoot Method in De Sitter Space

At this point, we present the overshoot/undershoot method in de Sitter space with dynamical gravity i.e. we do not assume the fixed background approximation. Of course, now, the shooting method is more difficult as we have to determine not only the initial value $\phi_0 = \phi(0)$ but also the final value $\phi_1 = \phi(\rho_{\max})$. The feature that makes this shooting method harder is that there are two coordinate singularities, $a(0) = 0$ and $a(\rho_{\max}) = 0$, from which the second one is movable. Note that, in order to avoid divergences, we have to impose $\dot{\phi} = 0$ at both of them.

Now, we describe the procedure for finding a bounce solution in de Sitter space with dynamical gravity which demands two shooting methods in both sides. At first, we choose arbitrary values for ϕ_0 and ϕ_1. The value of ϕ_0 has to be in the range $(\phi_{\rm fv}, \phi_{\rm bar})$ and the value of ϕ_1 has to be in the range $(\phi_{\rm bar}, \phi_{\rm tv})$. Afterwards,

we calculate two solutions ϕ_{true} and ϕ_{false} with the initial conditions $\phi_{\text{true}}(0) = \phi_1$, $\dot{\phi}_{\text{true}}(0) = 0$ and $\phi_{\text{false}}(0) = \phi_0$, $\dot{\phi}_{\text{false}}(0) = 0$. These two solutions do not satisfy the required boundary conditions.

Therefore, we use shooting method in both solutions as we described in section (3.4). Then, we match the two sides of the solution in order to find the entire solution. The point at which the two solutions connect can be chosen arbitrarily but here, we choose a point where $\dot{a}(\rho_{\text{mid}}) = 0$ which always exist as our solution in de Sitter space is compact.

Finally, we can compute $\rho_{\text{max}} = \rho_{\text{mid,true}} + \rho_{\text{mid,false}}$. The entire bounce solution is: $\phi_{\text{true}}(\rho)$ when ρ is between $(0,\ \rho_{\text{mid,true}})$ and $\phi_{\text{false}}(\rho_{\text{max}} - \rho)$ when ρ is between $(\rho_{\text{mid,true}},\ \rho_{\text{max}})$. We note that ϕ_{false} is flipped by the transformation $\rho \to \rho_{\text{max}} - \rho$ so as to match with ϕ_{true}. Similarly, we can calculate $a(\rho)$ and thus we are ready to calculate the action. This procedure helps us to avoid $a(\rho_{\text{max}}) = 0$ coordinate singularity as we integrate solutions from each side up to their middle. If this does not occur, we will integrate into a singularity and we will get an unstable numerical result.

5.2 Application to a Polynomial Potential

In this section, we apply the ideas of chapter 3 with dynamical gravity to a polynomial potential which has the following form

$$V(\phi) = -\frac{1}{2}\phi^2 + \frac{1}{4}\phi^4 - 0.1\phi + V_1, \tag{5.2.1}$$

where V_1 is a constant term. The true and the false vacuums as well as the position of the top of the barrier are again the same as in section (2.5) since the only difference between the two potentials is a constant term. We work once more in units that $M_P = 1$.

Firstly, we calculate the false-vacuum critical value but now we use the equation (3.3.2) as we consider gravitational back-reaction

$$V_{0\text{crit}} = 0.569369. \tag{5.2.2}$$

The corresponding critical Hubble rate is

$$H_{\text{crit}} = 0.435648. \tag{5.2.3}$$

Afterwards, we use the overshoot/undershoot method that was described in the previous section to solve these two equations of motion

$$\ddot{\phi} + \frac{3\dot{a}}{a}\dot{\phi} - V'(\phi) = 0, \tag{5.2.4}$$

$$\dot{a} = \sqrt{1 - \frac{a^2}{3M_P^2}\Big(- \frac{\dot{\phi}^2}{2} + V(\phi)\Big)}, \tag{5.2.5}$$

where dots represent differentiation with respect to the radial coordinate ρ. Note that, we choose the positive root in the latter equation. In this way, we calculate the solution up to ρ_{mid} where $\dot{a}(\rho_{\text{mid}}) = 0$. Knowing ρ_{mid}, we can modify the equation (5.2.5)

$$\dot{a} = \text{sgn}(\rho_{\text{mid}} - x)\sqrt{1 - \frac{a^2}{3M_P^2}\Big(- \frac{\dot{\phi}^2}{2} + V(\phi)\Big)}, \tag{5.2.6}$$

where sgn(x) is the sign function, which is -1 for negative numbers and +1 for positive numbers. Consequently, using the shooting method in both sides, we determine $\phi_0 = \phi(0)$ and $\phi_1 = \phi(\rho_{\text{max}})$ for each solution. Finally, we match together the solutions and we get entire CdL solutions for various values of false-vacuum potential V_0. These solutions are illustrated in figure 5.2.1.

Again, we conclude that the amplitude of CdL solutions decreases as V_0 increases. In the limit of $V_0 \to V_{0\text{crit}}$ from below, the amplitude of CdL solutions

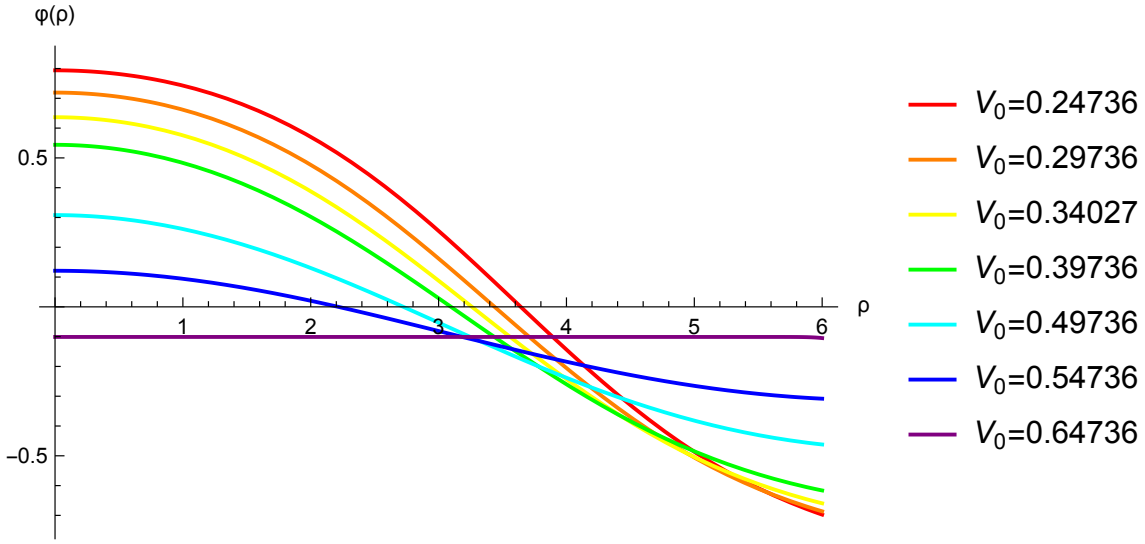

FIGURE 5.2.1: CdL solutions for various values of V_0 of the polynomial potential (5.2.1) with gravitational back-reaction

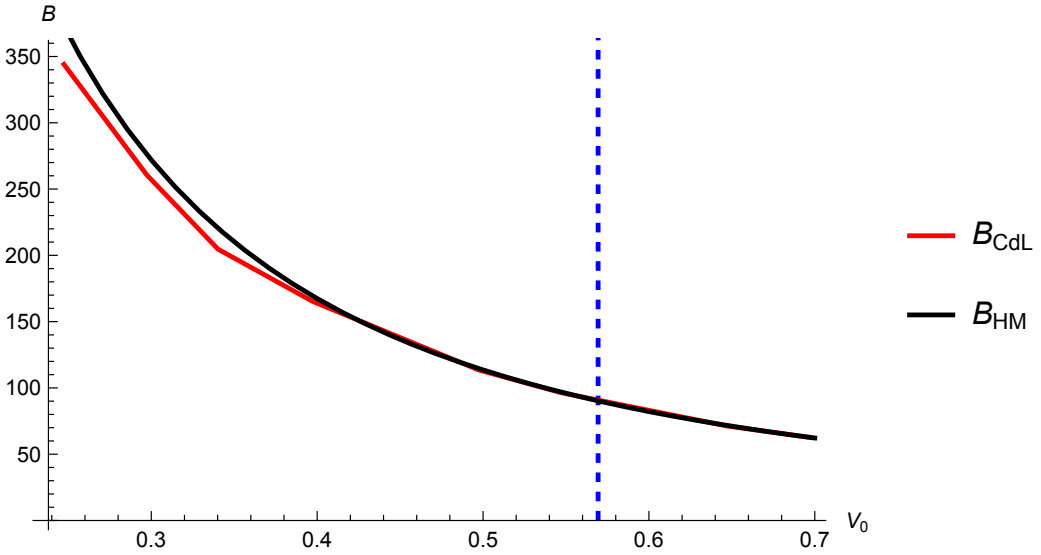

FIGURE 5.2.2: Decay exponent B vs false-vacuum potential V_0 graph with gravitational back-reaction. The dashed blue vertical line indicates the position of $V_{0\text{crit}}$.

tends smoothly to zero and thus CdL solutions approach the constant Hawking-Moss solution. An other important conclusion is that there are no CdL solutions above the critical threshold of the false-vacuum potential.

We also compute the decay exponents B for a given false-vacuum potential V_0. Figure 5.2.2 represents the relation between the decay exponent B and false-vacuum potential V_0 while figure 5.2.3 indicates the difference between B of the

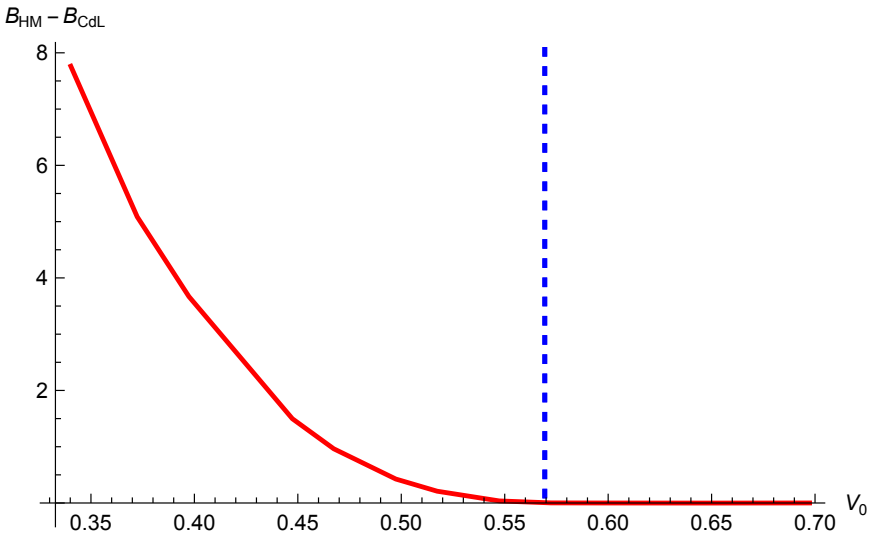

FIGURE 5.2.3: Difference between the decay exponent of Hawking-Moss solution and CdL solution vs false-vacuum potential V_0 graph with gravitational back-reaction. The dashed blue vertical line indicates the position of $V_{0\text{crit}}$.

Hawking-Moss solution and B of CdL solution for a specific value of V_0. The dashed blue vertical line indicates the position of $V_{0\text{crit}}$.

We notice once more that the decay exponent B of CdL solution merges smoothly with the decay exponent B of Hawking-Moss solution when we approach the critical threshold from below. We verify this with figure 5.2.3 since the difference between these two decay exponents B tends smoothly to zero when $V_0 \to V_{0\text{crit}}$.

The important conclusion of this section is that when we have gravitational back-reaction, above H_{crit}, there are no CdL solutions and thus Hawking-Moss solution dominates. Below the critical threshold, CdL solutions dominate. This conclusion is the same as the conclusion of the case of a fixed background.

Chapter 6

When is Dynamical Gravity Necessary?

In this last chapter, varying some parameters of the potential, we compare the solutions with a fixed de Sitter background with the solutions with dynamical gravity. When we use the fixed background approximation, there is no actual gravitational interaction with our solutions but in the dynamical gravity case, there is. Noticing these comparisons, we can conclude when dynamical gravity is necessary and when the fixed background approximation is a good approximation.

To study the impact of gravity on the nucleation rate of a bubble of true vacuum, we consider the following polynomial potential:

$$V(x) = ax^4 + bx^2 + cx + d, \tag{6.0.1}$$

where a, b, c and d are four parameters that allows to explore all possible cases.

In the first section, we vary only the parameter d so as to vary the false vacuum potential V_0 and thus we compare the decay exponents B of fixed de Sitter background with the decay exponents B with dynamical gravity for a given

V_0. In the second section, we vary the parameters c and d in order to vary the difference ΔV between the false vacuum potential and the potential at the top of the barrier and keep the V_0 constant. Then, we compare the decay exponents B of fixed de Sitter background with the decay exponents B with dynamical gravity for a given ΔV. Finally, in the last section, we end up with some important conclusions.

6.1 Decay Exponent B vs False Vacuum Potential V_0

In this case, the potential has the following form

$$V(x) = \frac{1}{4}x^4 - \frac{1}{2}x^2 - 0.1x + d, \tag{6.1.1}$$

where d is a constant. We vary this constant so as to vary the false vacuum potential V_0. The positions of the true and false vacuums and the position of the top of the barrier are the same for all values of V_0.

At first, we notice from the equation of the critical Hubble rate of a fixed de Sitter background and from the equation of the critical Hubble rate of a dynamical background

$$H^2_{\rm crit} = \frac{V_{0\rm crit}}{3M_P^2} = -\frac{V''(\phi_{\rm HM})}{4}, \tag{6.1.2}$$

$$H^2_{\rm crit} = \frac{V_{0\rm crit}}{3M_P^2} = -\frac{V''(\phi_{\rm HM})}{4} - \frac{[V(\phi_{\rm HM}) - V_0]}{3M_P^2} \tag{6.1.3}$$

that the critical Hubble rate and the critical potential of the false vacuum are constant when we vary the false vacuum potential V_0.

The numerical value of the false-vacuum critical value with a fixed de Sitter background is

$$V_{0\text{crit}} = 0.727034 \tag{6.1.4}$$

and the numerical value of the false-vacuum critical value with dynamical background is

$$V_{0\text{crit}} = 0.569369. \tag{6.1.5}$$

The latter value is smaller than the former as in the equation (6.1.3), there is an extra negative term which reduces the false-vacuum critical value. Therefore, we conclude that when we ignore dynamical gravity, we overestimate the false-vacuum critical value.

At this point, we plot graphs that illustrate the relation between the decay exponents B and V_0 with and without gravitational back-reaction. From figure 6.1.1, we note that when V_0 increases, the difference between the decay exponent B of Hawking-Moss solution with fixed background and with dynamical background decreases. This verifies the following expression

$$B_{\text{fg}} - B_{\text{dg}} = 24\pi^2 M_P^4 \, \frac{\Delta V(\phi_{\text{HM}})}{V_0}\left(\frac{1}{V_0} - \frac{1}{V(\phi_{\text{HM}})}\right), \tag{6.1.6}$$

and

$$\frac{B_{\text{fg}} - B_{\text{dg}}}{B_{\text{dg}}} = \frac{\Delta V(\phi_{\text{HM}})}{V_0}, \tag{6.1.7}$$

where B_{dg} and B_{fg} are the decay exponents of the Hawking-Moss solution with and without gravitational back-reaction, respectively.

From figure 6.1.2, we notice that the difference between the decay exponent B of CdL solution with fixed background and with dynamical background stays almost constant.

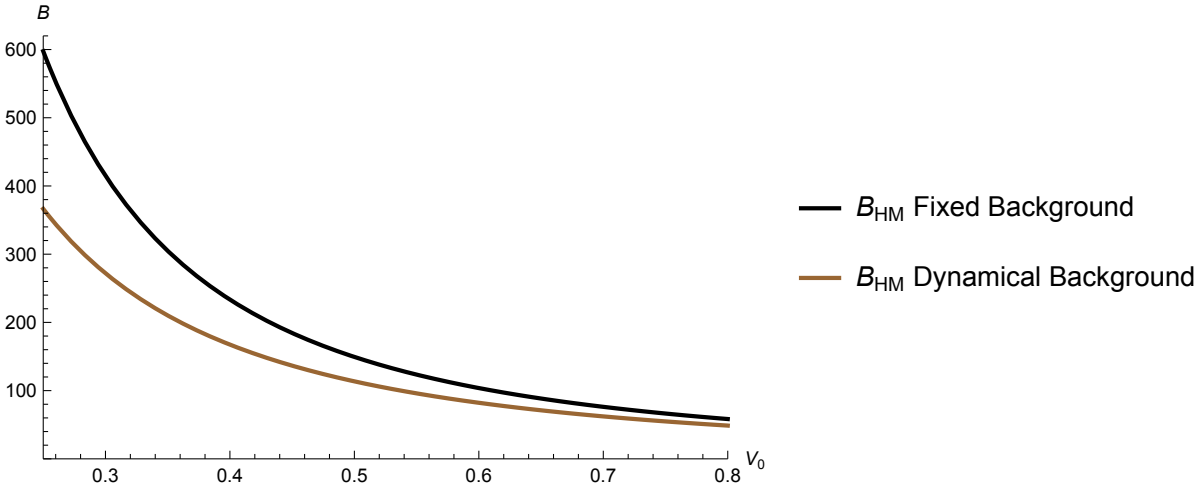

FIGURE 6.1.1: Decay exponent B of Hawking-Moss solution vs false-vacuum potential V_0 graph with and without gravitational back-reaction

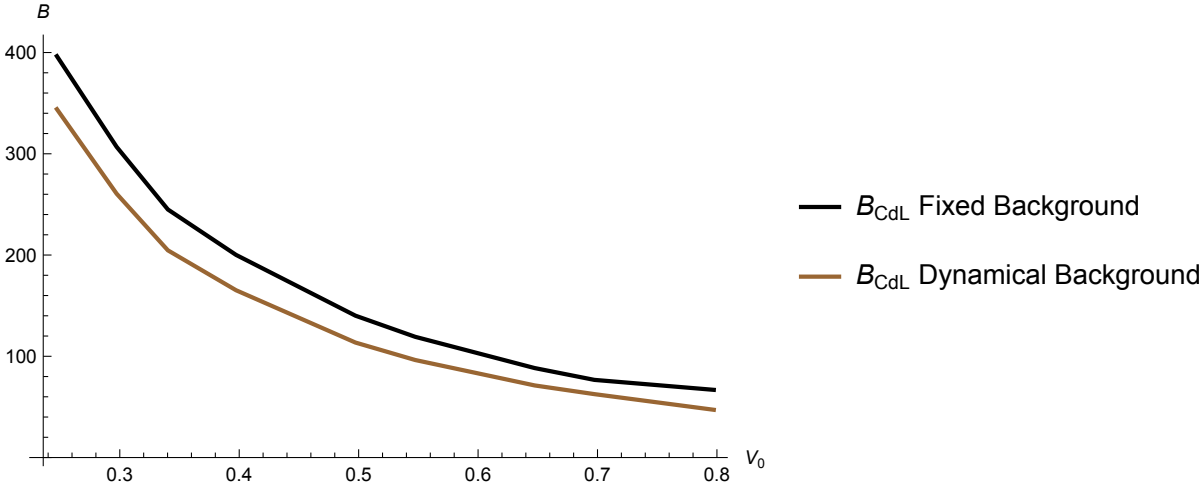

FIGURE 6.1.2: Decay exponent B of CdL solution vs false-vacuum potential V_0 graph with and without gravitational back-reaction

6.2 Decay Exponent B vs Difference ΔV between False Vacuum Potential and Potential at the Top of the Barrier

Now, the potential has the following form

$$V(x) = \frac{1}{4}x^4 - \frac{1}{2}x^2 - cx + d, \tag{6.2.1}$$

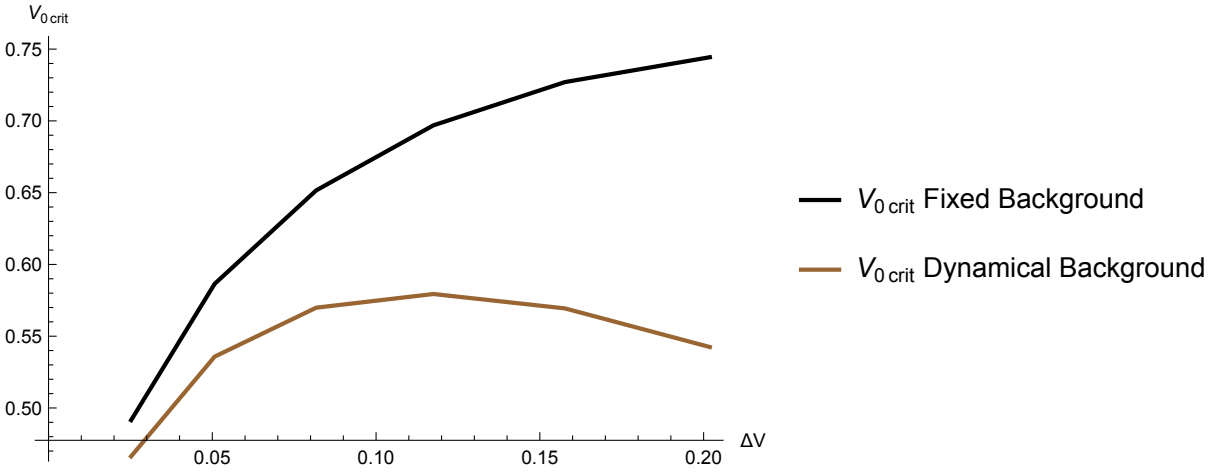

FIGURE 6.2.1: False-vacuum critical values $V_{0\mathrm{crit}}$ vs ΔV graph with and without gravitational back-reaction

where c and d are constants. We vary these two constants so as to vary the difference ΔV and keep the false vacuum potential V_0 constant. In this case, we calculate the positions of true and false vacuums and the position of the top of the barrier for each value of ΔV since they are different.

Firstly, we present the relation between the false-vacuum critical value $V_{0\mathrm{crit}}$ and the difference ΔV for the cases with and without gravitational back-reaction. This relation is shown in figure 6.2.1. We observe that the two false-vacuum critical values $V_{0\mathrm{crit}}$ deviate from each other while the difference ΔV increases. Consequently, we conclude again that when we ignore dynamical gravity, we over-estimate the false-vacuum critical value.

Afterwards, we plot graphs that demonstrate the relation between the decay exponents B and ΔV with and without gravitational back-reaction. From figure 6.2.2, we notice that when ΔV decreases, the difference between the decay exponent B of Hawking-Moss solution with fixed background and with dynamical background decreases. This verifies once more the following expression

$$\frac{B_{\mathrm{fg}} - B_{\mathrm{dg}}}{B_{\mathrm{dg}}} = \frac{\Delta V(\phi_{\mathrm{HM}})}{V_0}, \tag{6.2.2}$$

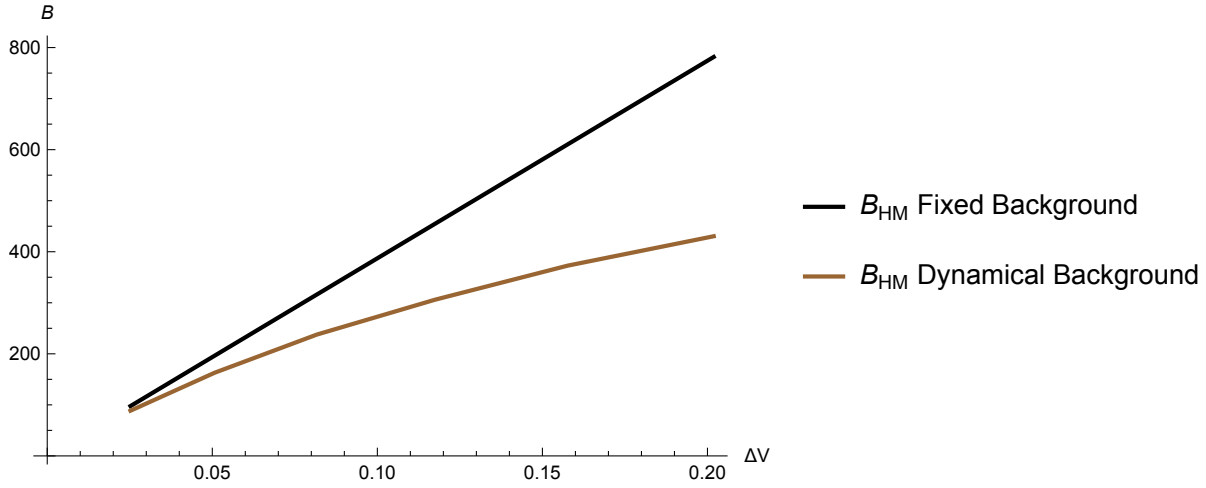

FIGURE 6.2.2: Decay exponent B of Hawking-Moss solution vs ΔV graph with and without gravitational back-reaction

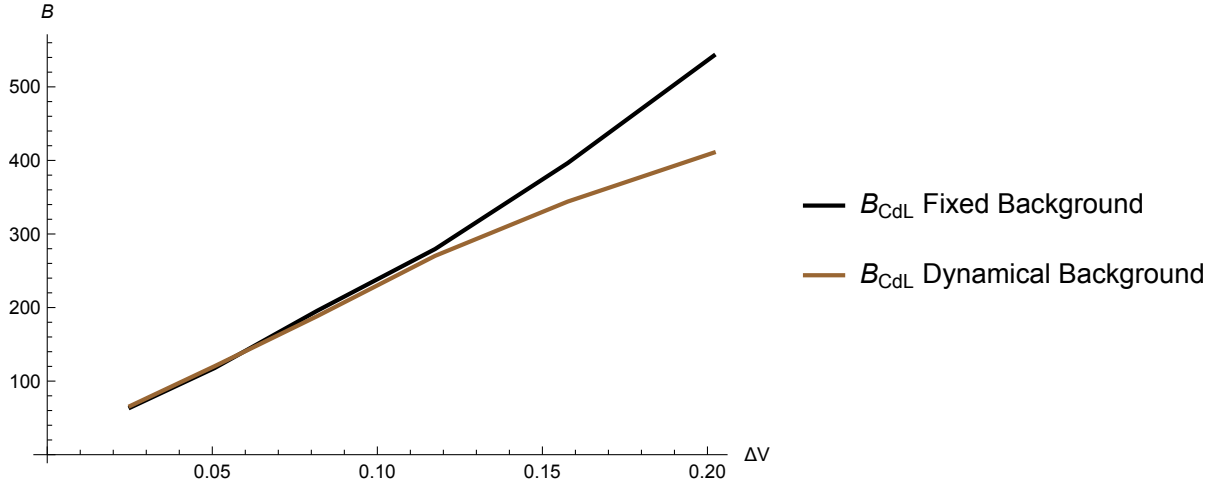

FIGURE 6.2.3: Decay exponent B of CdL solution vs ΔV graph with and without gravitational back-reaction

where B_{dg} and B_{fg} are the decay exponents of the Hawking-Moss solution with and without gravitational back-reaction, respectively.

From figure 6.2.3, we observe that when ΔV increases, the two curves of the decay exponents B of CdL solutions deviate from each other.

6.3 Conclusions

In this section, we present the conclusions from the observations of the last two sections.

One big question is when does dynamical gravity become important? For instance, Coleman and De Luccia proved that when the gravitational effects are weak, the probability of materialization of a true vacuum bubble is close to the flat space-time result. However, a strong gravitational field can stabilize the false vacuum, preventing the formation of true vacuum bubbles. These results are investigated when the energy density difference ΔV is small, the thin-wall regime. Here, we vary this ΔV to understand more than this as we know that the Standard Model does not fulfill the condition of small ΔV [14].

Importantly, we conclude that the false vacuum potential V_0 does not give us any clue whether the dynamical gravity is necessary or not. Varying the false vacuum potential V_0, we observe from figure 6.1.2 that we have a constant significant difference between CdL solutions with and without back-reaction. Since this difference is constant, we can conclude that we should vary other parameters to investigate when gravitational effects are important.

Therefore, we subsequently vary the difference ΔV which can be considered as the difference of the energy density. From figures 6.2.2 and 6.2.3, we conclude that the higher the value of energy density difference ΔV is, the stronger the gravitational effect is. Consequently, dynamical gravity is necessary when the value of the energy density difference ΔV is significantly large. In contrast, when the value of the energy density difference ΔV is small compared to the value of the false-vacuum potential V_0, background fixed approximation is a good approximation.

Observing the two figures 6.2.2 and 6.2.3, we can also conclude that when we ignore dynamical gravity, we overestimate the value of decay exponent B and thus, we underestimate the decay rate. In other words, including dynamical gravity enhances the decay rate i.e. increases the probability for the false vacuum decay. This situation is clearer when the energy density difference ΔV is much larger of the value of the false-vacuum potential V_0.

For instance, noticing the large depth of the Standard Model effective potential for the Higgs mass $M_h = 125.09 \pm 0.25$ GeV and the top quark mass $M_t = 173.21$ GeV, we conclude that the fixed background approximation does not hold. For this reason, if we want to calculate the bounce solutions, we should include all these back-reaction effects, without assuming that the metric is a fixed de Sitter background. Thus, it is worthwhile understanding these gravitational corrections that we calculate, even if we expect that ultimately new physics will change the situation. From the point of view of the future state of the universe, this is significantly important since the large negative Ricci curvature leads to a collapsing AdS region with a big-crunch like singularity. This effect cannot be predicted using a fixed background approximation [21].

The gravitational back-reaction is also relevant during inflation as the depth of the Standard Model vacuum, at least that reached by vacuum bubbles in flat space, is far larger than the cosmological constant [21].

Possible Future Directions

In this thesis, we calculate the results when the reduced Planck mass is equal to 1 ($M_P = 1$). For a future extent of this thesis, we can vary the value of M_P and see if we have the same conclusions for different energy scales. We can also add to the potential higher powers of the Higgs field (e.g. ϕ^6 and ϕ^8) and a fermionic and bosonic field with large masses. In this way, we will detect if the presence of new physics can have an impact on the vacuum stability condition [46]. Last but

not least, a term like $\frac{1}{2}\xi\phi^2 R$ can be added to the action so we can investigate if the nonminimal coupling ξ between the scalar field and gravity will affect when dynamical gravity is necessary.

Appendix A

The Semi-classical Approximation

When we refer to semiclassical physics, we mean that one part of a system can be described classically and the other part can be described quantum mechanically. There is also an approximation technique, which is called the semi-classical approximation as the wave function is written as an asymptotic series with ascending powers of the Planck constant, h, with the first term being purely classical.

We can use this technique to evaluate this integral:

$$\int D\phi e^{-S[\phi]} \tag{A.0.1}$$

having in our minds that the semi-classical approximation assumes that the path integral is dominated by classical solutions called instantons, or bounces, which are stationary points of the Euclidean action. Firstly, we expand the action around the instanton, $\phi = \phi_B + \eta$:

$$\int D\phi e^{-S[\phi]} \approx \int D\eta \exp\Big(- S[\phi_B] - \frac{1}{2}\int d^4x \int d^4y \ \eta(x) \frac{\delta^2 S[\phi_B]}{\delta\phi(x)\delta\phi(y)} \eta(y) + ... \Big). \tag{A.0.2}$$

We know that:

$$\frac{\delta S[\phi_B]}{\delta\phi(x)} = 0 \tag{A.0.3}$$

since ϕ_B is a stationary point of the Euclidean action. We also neglect higher order terms in (A.0.2) as they give small corrections. Then, we expand $\eta(x)$ in terms of the eigenfunctions of $\frac{\delta^2 S[\phi_B]}{\delta\phi(x)\delta\phi(y)}$:

$$\begin{aligned}&\int D\eta \exp\Big(-\frac{1}{2}\int d^4x \int d^4y\ \eta(x)\frac{\delta^2 S[\phi_B]}{\delta\phi(x)\delta\phi(y)}\eta(y)\Big) \\ &= \int D\eta \exp\Big(-\frac{1}{2}\int d^4x \int d^4y \sum_{n,m}\ c_n c_m \delta\phi_n(x)\frac{\delta^2 S[\phi_B]}{\delta\phi(x)\delta\phi(y)}\delta\phi_m(y)\ \Big).\end{aligned} \tag{A.0.4}$$

Now, we use the eigenvalue equation:

$$\frac{\delta^2 S[\phi_B]}{\delta\phi(x)\delta\phi(y)}\delta\phi_m(y) = \delta^{(4)}(x-y)\lambda_m\delta\phi_m(y) \tag{A.0.5}$$

and the orthogonality of the eigenfunctions in order to evaluate the integral:

$$\begin{aligned}&\int D\eta \exp\Big(-\frac{1}{2}\int d^4x \int d^4y \sum_{n,m}\ c_n c_m \delta\phi_n(x)\delta^{(4)}(x-y)\lambda_m\delta\phi_m(y)\ \Big) \\ &= N\prod_n\Big(\int dc_n e^{-\frac{\lambda_n c_n^2}{2}}\Big),\end{aligned} \tag{A.0.6}$$

where N is the ratio between the two measures: $D\eta$ and $\prod_n dc_n$.

Finally, knowing the result:

$$\int_{-\infty}^{\infty} dc_n e^{-\frac{\lambda_n c_n^2}{2}} = \sqrt{\frac{2\pi}{\lambda_n}}\ , \tag{A.0.7}$$

we can calculate the functional integral:

$$\int D\phi e^{-S[\phi]} \approx N e^{-S[\phi_B]}\prod_n\left(\frac{2\pi}{\lambda_n}\right)^{\frac{1}{2}} = N\ \det\left(\frac{S''[\phi_B]}{2\pi}\right)^{-\frac{1}{2}} e^{-S[\phi_B]}. \tag{A.0.8}$$

It is worth noted that this result is infinite as the path integral diverges. Therefore, we consider only ratios of functional determinants.

Bibliography

[1] Aad G., Abajyan T., Abbott B., Abdallah J., Khalek S. A., Abdelalim A., Abdinov O., Aben R., Abi B., and Abolins M. et al. Observation of a new particle in the search for the Standard Model Higgs boson with the ATLAS detector at the LHC. In: *Phys. Lett. B 716, 1* (2012).

[2] Chatrchyan S., Khachatryan V., Sirunyan A., Tumasyan A., Adam W., Aguilo E., Bergauer T., Dragicevic M., Er J., and Fabjan C. et al. Observation of a new boson at a mass of 125 GeV with the CMS experiment at the LHC. In: *Phys. Lett. B 716, 30* (2012).

[3] M. Sher. Electroweak Higgs potential and vacuum stability. In: *Phys. Rep. 179, 273* (1989).

[4] K. A. Olive et al. Review of Particle Physics. In: *Chin. Phys. C 38, 090001* (2014).

[5] Degrassi G., Di Vita S., Elias-Miró J., Espinosa J. R., Giudice G. F., Isidori G., and Strumia A. Higgs mass and vacuum stability in the Standard Model at NNLO. In: *J. High Energy Phys. 08 098* (2012).

[6] Buttazzo D., Degrassi G., Giardino P. P., Giudice G. F., Sala F., Salvio A., and Strumia A. Investigating the near-criticality of the Higgs boson. In: *J. High Energy Phys. 12 089* (2013).

[7] A. Kobakhidze and A. Spencer-Smith. Electroweak vacuum (in)stability in an inflationary universe. In: *Phys. Lett. B 722, 130* (2013).

[8] Branchina V., Messina E., and Platania A. Top mass determination, Higgs inflation, and vacuum stability. In: *J. High Energy Phys. 09 182* (2014).

[9] M. Fairbairn and R. Hogan. Electroweak Vacuum Stability in Light of BICEP2. In: *Phys. Rev. Lett. 112, 201801* (2014).

[10] Herranen M., Markkanen T., Nurmi S., and Rajantie A. Spacetime Curvature and the Higgs Stability During Inflation. In: *Phys. Rev. Lett. 113, 211102* (2014).

[11] Herranen M., Markkanen T., Nurmi S., and Rajantie A. Spacetime Curvature and Higgs Stability after Inflation. In: *Phys. Rev. Lett. 115, 241301* (2015).

[12] S. Coleman and F. De Luccia. Gravitational effects on and of vacuum decay. In: *Phys. Rev. D 21, 3305* (1980).

[13] Isidori G., Rychkov V. S., Strumia A., and Tetradis N. Gravitational corrections to standard model vacuum decay. In: *Phys. Rev. D 77, 025034* (2008).

[14] Branchina V., Messina E., and Zappala D. Impact of gravity on vacuum stability. In: *EPL 116 21001* (2016).

[15] Gregory R., Moss I. G., and Withers B. Black holes as bubble nucleation sites. In: *J. High Energy Phys. 03 081* (2014).

[16] Burda P., Gregory R., and Moss I. G. Vacuum metastability with black holes. In: *J. High Energy Phys. 08 114* (2015).

[17] Burda P., Gregory R., and Moss I. G. The fate of the Higgs vacuum. In: *J. High Energy Phys. 06 025* (2016).

[18] C. G. Callan and S. Coleman. Fate of the false vacuum. ii. first quantum corrections. In: *Phys. Rev. D16, 1762* (1977).

[19] S. Coleman. Fate of the false vacuum: Semiclassical theory. In: *Phys. Rev. D15, 2929* (1977).

[20] S. Coleman. *Aspects of symmetry.* Cambridge University Press, 1985. ISBN: 9780511565045.

[21] Stephen Stopyra. "Standard Model Vacuum Decay with Gravity". PhD thesis. Imperial College London, 2018.

[22] Buttazzo D., Degrassi G., Giardino P. P., Giudice G. F., Sala F., Salvio A., and Strumia A. Investigating the near-criticality of the Higgs boson. In: *J. High Energy Phys. 12 089* (2013).

[23] Alekhin S., Djouadi A., and Moch S. The top quark and Higgs boson masses and the stability of the electroweak vacuum. In: *Phys. Lett. B 716, 214* (2012).

[24] Degrassi G., Di Vita S., Elias-Miró J., Espinosa J. R., Giudice G. F., Isidori G., and Strumia A. Higgs mass and vacuum stability in the Standard Model at NNLO. In: *J. High Energy Phys. 08 098* (2012).

[25] Coleman S., Glaser V., and Martin A. Action minima among solutions to a class of Euclidean scalar field equations. In: *Commun. Math. Phys. 58, 211* (1978).

[26] A. Rajantie and S. Stopyra. Standard model vacuum decay with gravity. In: *Phys. Rev. D 95, 025008* (2017).

[27] Salvio A., Strumia A., Tetradis N., and Urbano A. On gravitational and thermal corrections to vacuum decay. In: *J. High Energy Phys. 09 054* (2016).

[28] Espinosa J. R., Fortin J.-F., and M. Trpanier. Consistency of scalar potentials from quantum de Sitter space. In: *Phys. Rev. D 93, 124067* (2016).

[29] Masoumi A., Paban S., and Weinberg E. J. Tunneling from a Minkowski vacuum to an AdS vacuum: A new thin-wall regime. In: *Phys. Rev. D 94, 025023* (2016).

[30] V. A. Rubakov and S. M. Sibiryakov. False vacuum decay in de Sitter spacetime. In: *Theor. Math. Phys. 120 1194* (1999).

[31] A. Rajantie and S. Stopyra. Standard model vacuum decay in a de Sitter background. In: *Phys. Rev. D 97, 025012* (2018).

[32] Isidori G., Ridolfi G., and Strumia A. On the metastability of the Standard Model vacuum. In: *Nucl. Phys. B609, 387* (2001).

[33] G. W. Gibbons and S. W. Hawking. Action integrals and partition functions in quantum gravity. In: *Phys. Rev. D 15, 2752* (1977).

[34] Masoumi A., Paban S., and Weinberg E. J. Tunneling from a Minkowski vacuum to an AdS vacuum: A new thin-wall regime. In: *Phys. Rev. D 94, 025023* (2016).

[35] J. Garriga and A. Megevand. Decay of de Sitter Vacua by Thermal Activation. In: *Int. J. Theor. Phys. 43, 883* (2004).

[36] A. Masoumi and E. J. Weinberg. Bounces with O(3)×O(2) symmetry. In: *Phys. Rev. D 86, 104029* (2012).

[37] S. Hawking and I. Moss. Supercooled phase transitions in the very early universe. In: *Phys. Lett. 110B, 35* (1982).

[38] A. R. Brown and E. J. Weinberg. Thermal derivation of the Coleman-De Luccia tunneling prescription. In: *Phys. Rev. D 76, 064003* (2007).

[39] J. C. Hackworth and E. J. Weinberg. Oscillating bounce solutions and vacuum tunneling in de Sitter spacetime. In: *Phys. Rev. D 71, 044014* (2005).

[40] S. Coleman. Quantum tunneling and negative eigenvalues. In: *Nucl. Phys. B298, 178* (1988).

[41] G. Lavrelashvili. Number of negative modes of the oscillating bounces. In: *Phys. Rev. D73, 083513* (2006).

[42] Battarra L., Lavrelashvili G., and Lehners J.-L. Negative modes of oscillating instantons. In: *Phys. Rev. D86, 124001* (2012).

[43] S. Gratton and N. Turok. Homogeneous modes of cosmological instantons. In: *Phys. Rev. D 63, 123514* (2001).

[44] V. Balek and M. Demetrian. Euclidean action for vacuum decay in a de Sitter universe. In: *Phys. Rev. D71, 023512* (2005).

[45] V. Balek and M. Demetrian. Criterion for bubble formation in a de Sitter universe. In: *Phys. Rev. D 69, 063518* (2004).

[46] Bentivegna E., Branchina V., Continoa F., and D. Zappal. Impact of new physics on the EW vacuum stability in a curved spacetime background. In: *J. High Energy Phys. 12 100* (2017).